Journal of Radiation and Nuclear Applications
An International Journal

http://dx.doi.org/10.18576/jrna/070208

Geology, Radioactivity and Mineralogy of Granitic Rocks and Silica Veins of El-Erediya area, Central Eastern Desert, Egypt

Nasser M. Moghazy[*]

Nuclear Materials Authority, P.O. 530 Maadi, Cairo, Egypt.

Received: 21 Feb. 2022, Revised: 22 Mar. 2022, Accepted: 24 Mar. 2022.
Published online: 1 May 2022.

Abstract: This work discusses the geology, geochemistry, distribution of the natural radionuclides and the mineralogical studies of the radioactive minerals in El Erediya granites, Central Eastern Desert, Egypt. EI-Erediya syenogranite mass showing characteristic higher topography than the surrounding rocks. It is oval shaped, elongated in NW-SE direction and dissected with numerous sub-parallel shear zones trending NE-SW in the southwestern part of the G. El Erediya. The pluton is characterized by different degrees of alterations comprises silicification, hematitization, sericitization (± minor greisenization), kaolinization as well as jasper and quartz veins. The uranium mineralization is closely associated with Jasper veins, varying in thickness of 20 cm in average and length from few meters to more than 100 meters within the granites and with no extensions to the surrounding country rocks. U-mineralization encountered in jasper veins and veinlets are believed to be of magmatic and hydrothermal origin after the emplacement, contraction and fracturing of the crystallized magma.

Geochemically, the studied granites are true granites in composition and characteristics and most probably originated from high K calc-alkaline magma. The studied granites predominantly show metaluminous to slightly peraluminous nature and syenogranites are A-type granites and belonging to A_2 group which represents magmas derived from continental crust or under-plated crust that has been subjected to a cycle of continent- continent collision or island-arc magmatism. The El Erediya granites were developed in within plate tectonic setting and derived from tonalite magmas or crustal sources under pressure varying between (2->5kb) and temperatures of crystallization ranging from 820^o to 840^o c, emplaced at moderate depths >30 km and the crystal fractionation was the predominant process during magmatic differentiation. Hydrothermal alterations are common in the form of silicification, hematitization, sericitization , greisenization and kaolinitization.

Radiometricaly, we may concluded that the syenogranites are considered as anomalous granites and the silica veins as fertile rocks. Also, a magmatic and strong post-magmatic condition play an important role in the distribution of uranium in the studied rocks. The uranium and thorium contents are encountered in uranium and thorium minerals as well as radioactive bearing minerals as uranophane, autonite, uranothorite, thorite, columbite, xenotime, zircon, monazite, sphene, fluorite, allanite and apatite.

Keywords: El Erediya, Syenogranite, Silicification, Uranophane.

1 Introduction

The Arabian-Nubian Shield (ANS), forming considerable parts of NE Africa and Arabia, as juvenile continental crust that had evolved between 900 and 550 Ma. The evolution of the ANS encompasses four major tectono-magmatic episodes that occurred between 900 and 550 Ma, 1)- intra-oceanic arc magmatism (900–700 Ma), 2)- accretion of arc complexes resulting in closure of the Mozambique Ocean (~800–650 Ma), 3)- eventual collision between West and East Gondwana blocks, 4)- followed by collapse of the thickened crust, and the associated strike-slip faulting, extension and delamination (630–550 Ma) [1-9]. Pre-Neoproterozoic crust (Paleoproterozoic or Archean) is tectonically intercalated with the Neoproterozoic rocks in the eastern, western and southern ANS. [10] reported Rb-Sr age for El-Erediya granite is 570 Ma, while U-Pb age is about 583 Ma [11]. These ages confirm the coeval emplacement of the investigated granite masses as part of a huge massif during the post tectonic epidose (603-575 Ma.) at the culmination of Pan-African thermo-tectonic event [12].

The Arabian Nubian Shield (ANS) is regarded the best preserved and largest exposed area of Neoproterozoic juvenile continental crust on the Earth [2, 7, 13]. In the northern ANS, including the Eastern Desert (ED) of Egypt

[*]Correspondingauthore-mail: nassmoghazy@yahoo.com

and Sinai, granitoids represent around 50% of the exposed basement [14-17], while more to the south in Sudan and Ethiopia, the exposures are about 30% of the entire outcrop [15]. Within the Egyptian part, the dominance of granitoids increases northward attaining the highest abundance (~70% of the overall basement area) in Sinai, and even in the entire ANS [18, 19].

The Egyptian granitoids are of I- and A- type affinity, and were generated either by partial melting of mafic lower crust or by fractionation of a mantle-derived magma [20-22]. Recently, [23] classified the younger granitoids into orogenic I-type arc-related, orogenic A-type arc-related, and anorogenic A-type rift-related granites. Most of the geological work on the younger granitoids in Egypt dealt with the arc-related types and little attention has been given to the post-orogenic and anorogenic granitoids [24, 25].

The common Egyptian uranium occurrences are mainly: vein type (G. El-Missikat and G. El-Erediya [26, 27], G. Sella [28, 29], metasomatised granites (G. Um Ara [30], shear zones in calc-alkaline granite (G Gattar [31], and shear zones hosted lamprophyre bearing-REEs and U in Abu Rusheid area [32]. Uranyl silicates are typical alteration phases of the primary uranium mineralization of the alteration zone of many uranium deposits. Uranyl silicate minerals are typical representatives of the long-term alteration products, indicating usually late stage, or the high-grade of weathering. Uranyl silicates, as uranophane and/or kasolite, are common constituents of massive aggregates of alteration phases, replacing primary uraninite in situ; aggregates of uranyl silicates occur often along with uranyl phosphates in the strongly oxidized portions of the primary mineralization [33]. Subsequent hydrogeological processes causing U solution, precipitation and geological phenomena such as faults, hydrothermal alterations and weathering can favor further local enrichment in a granitic environment [34-37] . Uranium mineralization in G. El Erediya, is structurally controlled and restricted to shear zones where uranium bearing minerals occur either as small veinlets or as minute dissemination associated with hydrothermal alteration within jasperoid veins related to granitic pluton. The origin of secondary uranium mineralization in El Erediya area has been previously related to the alteration of pitchblende [11, 38-41]. The uranium mineralization was recorded in the southern part of El Erediya granitic pluton [42]. Surface and subsurface geologic studies were carried out to develop and evaluate El Erediya uranium occurrence [11, 27, 43-47].

The present work is achieved through detailed geologic, petrographic, spectrometric, mineralogical and geochemical studies on the El Erediya granitic mass with paying a special attention to the most promising shear zone. Also, Tectonic regime combined with the description of alteration processes may help to understand high levels of radioactivity in El Erediya granitic pluton.

2 Geologic Setting

G. El Erediya younger granites is located in the central Eastern Desert of Egypt, south Qena-Safaga asphaltic road, covering about 25 km2 bounded between latitudes 26° 18' 36" - 26° 21' 36"N and longitudes 33° 27' 18" - 33° 30"E. (Fig. 1). This granite belongs to the post-orogenic younger granite magmatic activity that intruded the Egyptian shield between 620 and 530 Ma. According to the field geological study and the previous works, the basement exposures in the area arranged from the oldest to the youngest are metavolcanics, amphibolites, younger granites, pegmatites, aplites, jaspriod veins and basic dykes. These rocks were formed during the Neoproterozoic East Africa orogensis (900-550Ma) [18, 48, 49].

Metavolcanics represent the oldest rock type cropping out to the northeast of the study area. They are represented by metabasalts, meta-andesites, metarhyodacites and their pyroclastics. They are fine-grained and dark greenish to greenish black in color. They are intruded with granitic dykes and offshoots. Also, they are found as roof pendants and xenoliths in the younger granites. The amphibolites cover a small part in the area and form relatively low hills. They are hybrid rocks of variable composition and grade. They are present in the southeastern part of the mapped area as medium to coarse-grained and of green to grayish green colors. They are intruded by a large number of aplite dykes and offshoots of pink granite. They occur as roof pendants carried on the younger granite. A great part of these amphibolites are thermally metamorphosed, resulted due to the emplacement of the granitic intrusions, where the rocks along the contact zone become highly foliated.

The younger granites of the area under study represented by syenogranites (G. El Erediya). This granite showing characteristic higher topography than the surrounding rocks. It is oval shaped, elongated in NW-SE direction and sending apophyses and offshoots within the surrounding country rocks. The syenogranites is essentially medium to coarse-grained and composed of alkali feldspars, quartz and plagioclase, with minor amounts of mafics and opaque minerals. Numerous sub-parallel shear zones trending NE-SW dissect the southwestern part of the G. El Erediya pluton which are characterized by different degrees of alterations (Fig.2a). These hydrothermal alterations comprises silicification, hematitization, sericitization (± minor greisenization), kaolinization as well as jasper and quartz veins (Fig.2b,c and d).

Jasper veins, to which the uranium mineralization is closely associated, vary in thickness of 20 cm in average and length from few meters to more than 100 meters within younger granites and with no extensions to the surrounding country rocks (Fig.2e). Jasper is the last product of silicification of the granite in which the minerals are progressively replaced by jasper. U-mineralization encountered in jasper veins and veinlets are believed to be of magmatic hydrothermal origin after the emplacement, contraction and fracturing of the crystallized magma. The

fractures were filled with residual magmatic hydrothermal solutions forming pegmatites then jasper filling the fractures.

The younger granite around the jasper veins is highly silicified with a deep reddish color due to impregnation of the feldspars by liberated hematite. This effect fades out gradually away from the veins. The silicified granite zone is surrounded by a zone of kaolinized granite, which grades outwards into the fresh granite. The jasperoid veins are cracked, fractured and sometimes form brecciated fragments composed of jasper and granite cemented with final silica rich solutions with black shreds (Fig.2f).

Alteration aureoles exhibit a symmetrical pattern around the siliceous veins which reflect a sequential paragenetic formation. It is often possible to traverse these zones from siliceous vein or veinlet to fresh granite. The sequence at El Erediya area starts with silicification, hematitization, sericitization (± minor greisenization), and finalized by kaolinization.

Uranium mineralization is associated with the hydrothermally altered parts of the El Erediya granite and localized within several shear and fractured zones that are filled with jasperoid veins. Most of the radioactive veins are lined with continuous zones of alteration such as hematitization, sericitization and stains of manganese oxides.

Jasperoid silica has a deep-brownish red colour, (Fig. 2d) and is moderately to highly radioactive (900-4000 cps) and typically associated with U minerals (Fig. 2f).

The brownish, black red jasperoid silica are amorphous to cryptocrystalline. Brecciation is very common feature met with in the siliceous veins in which angular to sub-rounded fragments of light silica, fresh and altered granite frameworks are cemented by later black or brownish silica matrix. jasperoid veins developed at El Erediya exhibit a complex pattern of faulting and brecciation accompanying the enormous hematitization.

3 Methods and Techniques

In order to represent the various degrees of alteration of the El Erediya syenogranite, Forty samples were collected to cover the areal variation in petrographic and textural characteristics of the investigated granites and jasperoid veins. The perographic studies are carried out in Nuclear Materials Authority (NMA) laboratories using a Nikton (Optiphot-Pol) polarizing microscope equipped with a full automatic photomicrographic attachment (Microflex AFX-II). In addition, five selected fresh samples.

Uranium, thorium, radium and potassium contents are determined radiometrically by using a multichannel analyzer of γ -ray detector (Gamma Spectrometer technique). The instrument used in determination of the four radioactive elements consists of a Bicon scintillation detector NaI (TI) 76 mm X 76 mm, hermetically sealed with the photomultiplier tube in aluminum housing. The measurements involve determining the equivalent of U, Th, Ra (ppm) and K (%) concentrations using a high efficiency multichannel analyzer of gamma-ray spectrometer (NaI "T1" detector). The measurements were carried out in sample plastic containers, cylindrical in shape, 212.6 cm in volume with 9.5 cm average diameter and 3 cm height.

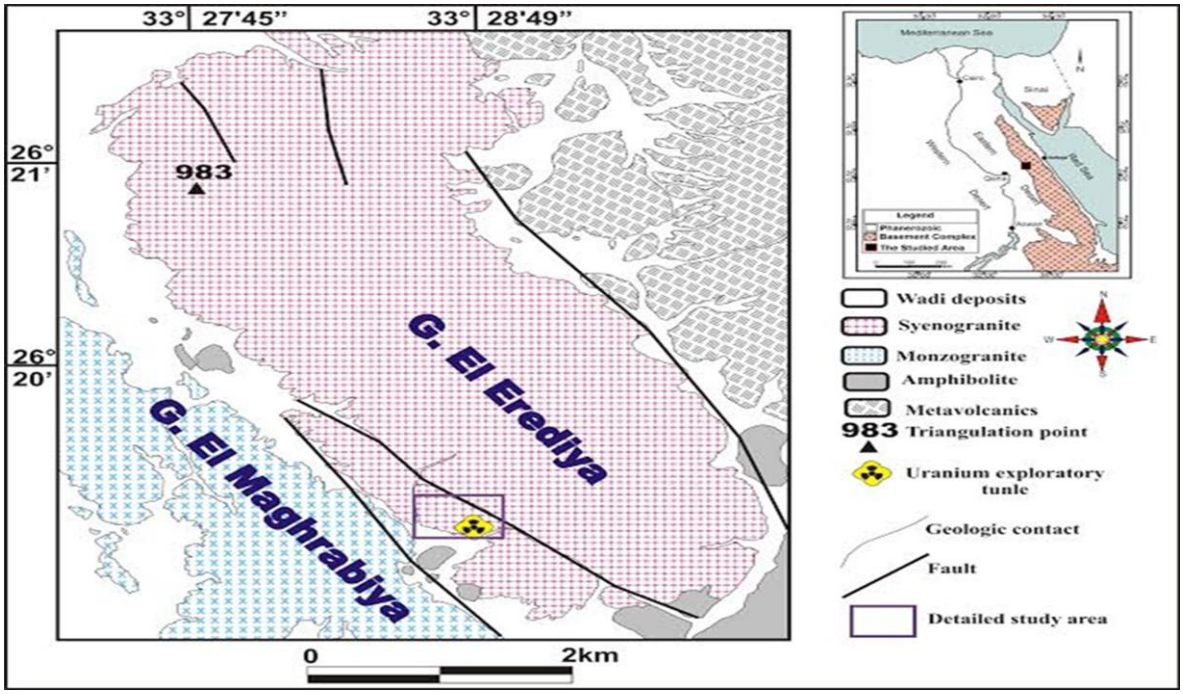

Fig. 1: Geologic map of El Erediya area, CED after [50].

The rock sample was crushed as fine as about 1 mm in grain size and the container was then filled with about 300 – 400 gm of the crushed sample sealed well and left for at least 21 days to accumulate free radon to attain radioactive equilibrium. The relation between the percentage of ^{222}Rn accumulations and time increased till reaching the steady stage after about 38 days [51].

Selected samples from the studied area were chosen on the basis of their high radioactivity levels for heavy minerals separation. The samples were crushed, ground, sieved and then were subjected to heavy liquid separation process using bromoform (sp.Gr. 2.89), to separate light and heavy fractions followed by removal of magnetite by hand magnet. The obtained fractions were carefully studied using a Binocular Stereomicroscope. Semi-quantitative (EDX) analyses and identification of the picked mineral were carried out using a Phillips XL 30 Scanning Electron Microscope (SEM) in the NMA Labs.

The quantitative analysis of selected samples was carried out by Inductively Coupled Plasma Mass Spectrometry (ICP-MS) at the Acme Labs, Vancouver, Canada. About 5 gm of the picked mineral was ground in an agate mortar to 200 mesh size. The samples were fused with LiBO2 digested and analyzed using the ICP-MS. The analytical precision monitored by international rock standards is found to be better than ±7% for rare earth elements (REE) and with 5-10% for trace elements and ±2% for major oxides.

4 Petrography

The younger granite of EI-Erediya pluton is massive with characteristic pink color and medium- to coarse-grained. It is essentially syenogranite composed of micocline perthite, quartz and plagioclase, with very subordinate amounts of biotite (Fig.3a) and opaque minerals. Potash are mainly represented by microcline and microcline perthites. The crystals are euhedral to subhedral of fine- to medium-grained. The perthites invaded by quartz and plagioclases as well as they are cracked, crushed and exhibit filament and feather types. Subhedral quartz crystals exhibit wavey extinction reflecting strain effect. Plagioclases are mostly present as small crystals between potash feldspar and quartz. Micas are represented by anhedral to subhedral biotites, phlogopite and rarely muscovite crystals. Biotite occurs as sub- to anhedral, medium-grained flakes of 3-5 mm length and is perchloric from yellowish-green to green, sometimes altered to chlorites (Fig. 3a). Mica minerals in altered varieties represent low percentage of the rock occurring as muscovite that occasionally associated with lithium mica (zinnwaldite). The latter occurs as orange flaky crystals enriched by iron oxides (Fig.3b,c). Generally, the granite shows various intesity of shearing comprising the brecciation and reworking of all rock forming minerals. Mechanically the rock is cataclazed and most of the quartz crystals are pulverized and fragmented forming the mortar texture or reworked to finer crystals (Fig.3 c,d,e and f). The crystals of potash feldspar are mostly fractured and sericitized or partially or completely silicified (Fig.3g, h).

The accessory minerals are represented by fluorite, zircon, autonite, metautonite (Fig. 4a,b) allanite (Fig. 4 c,d and e), and titanite which are dominant associated with micas. Zircon faintly metamictized and fractured by effect of the radioactive damage (Fig. 4f). The former occurs as well formed crystals of deep red color and translucent appearance showing its characteristic zoning in association with titanite (Fig. 4g,h). Epidote, chlorite, calcite, radioactive minerals (uranophane, beta-uranophane, kasolite and uranothorite) are secondary minerals.

These granites more or less suffered alteration, particularly along the fault planes and shear zones. The intensity of these alteration features increase gradually toward the shear zones especially those enriched by jasper veins. It is observed that the introduction of siliceous material during vein formation was accompanied by a contemporaneous silicification of the adjacent granite wallrock.

Hydrothermal alterations are common in the form of silicification (in the vicinity of vein), hematitization, sericitization (± minor greisenization) and concluded by kaolinitization. Jasperoid vein formation (i.e. jasperization) can be considered as the ultimate product of silicification of the granite in which the minerals are progressively replaced by silica gel (Jasper). It is presumably of the same age and is intimately related to the hematitization. Conspicuously, jasperization is not a wall-rock alteration but rather a process by which the jasper veins are formed.

Silicification is manifested by intensive impregnation of granite with the siliceous veins by medium- to coarse-grained quartz crystals which may indicate that the introduction of siliceous material during vein formation was contemporaneously accompanied by a silicification of the adjacent granite wallrock (Fig.3 c,d).

Hematitization is manifested by change of the pink colour of fresh granite into a deep blood-red colour due to impregnation of the granite-forming minerals by hematite dust. When the process becomes overwhelming, the feldspar laths are attached and totally replaced by dusty opaque mineral (hematite) and the granite becomes a crumbly mass of intense brick-red material (Fig.3b,c).

Sericitization is manifested by the development of fine-grained, green flakes of dioctahedral white micas (i.e. phengitic white mica) on expense of feldspars. Sericite is not markedly different from muscovites where they are reported to contain higher Si and Fe and lower Al [52]. The process of sericitizatiion involves consumption of H^+ and destabilization of feldspar, and instead fine-grained white mica and quartz are stably formed (Fig.3g,h).

Kaolinization is characterized by the development of kaolinite due to intense H^+ metasomatism (acid leaching). Zone of kaolinized granite grades outwards into fresh

granite and inwardly into sericitic zones. Quartz, kaolinite, and fine grained sericite are the dominant minerals in the kaolinized granite. The process grades from slight alteration of K-feldspar to an advanced stage where the rock becomes white and highly friable. Under high magnification, kaolinite occurs as finely crystalline euhedral plates of pseudohexagonal shapes along the relicts of cleavage planes and peripheries of corroded feldspar laths and white mica flakes (formed during the preceding sericitization event).

5 Geochemistry

Sixteen samples from EI-Erediya granites were selected and prepared for geochemical analysis of major oxides, trace and rare earth elements as shown in Table 1. The geochemical classifications of granitic rocks mainly follow [53] as shown in (Fig. 5A) the studied granite samples plot in the alkali feldspar granite field. Primitive mantle-normalized spider diagram [54] for the studied granites show higher than primitive mantle values among the most elements (Figs. 5B). The patterns of the studied granites show more enrichment in (HFSE) such as Nb, Zr, Th, U, Y and HREE with low contents of the compatible elements Sr and Ba and high to enhanced contents of the incompatible elements Zr, Y, Nb, U and Th coupled with negative Eu anomalies suggest a fractional geochemical signature for younger granites which is a typical feature of rare metal granites [55, 56]. The relative enrichment in the HREE (Tm, Yb and Lu) can be attributed to the presence of the high contents of xenotime and zircon which are traditionally known as HREE accumulators [57]. [58] Stated that the negative anomalies can be attributed to the fractionation of feldspars, apatite and Fe-Ti oxides. In addition to the Sr, P and Ti negative anomalies on the spider diagrams of granites, there is a strong negative Ba anomaly on the spider diagram of alkali feldspar granite.

Rare earth elements (REEs) are useful geochemical tool where they could give valuable information about rock genesis. REEs data for the studied granitic rocks (Table 1) are shown in chondrite-normalized diagrams (Fig. 5C). The average of total REE contents of the studied syenogranites are 188.66ppm suggesting that these granites are depleted in REE range (250-270) of [59].

In General, the REE patterns of the studied granites have a wing shape with $(La_n/Yb_{n)}$ values vary from 0.887 and 1.651. The difference in LREE abundances could be explained by crystal fractionation of minerals that prefer LREE. Fractionation of zircon, apatite and allanite could cause a reduction in LREE abundance due to their large partition coefficients for the REE [60]. The LREE/MREE values are moderate to high fractionated in the studied syenogranites (La_n/Sm_n =2.340 – 7.143).

The REE pattern of the syenogranite is closely similar and display strong negative Eu anomalies (Eu/Eu* = 0.26- 0. 38). The extremely negative Eu anomaly values in the syenogranites can be attributed to the removal of plagioclases from the source magma by fractional crystallization [61].

5.a. Magma and granitic types

The chemical nature and behavior of the magma during its evolution for the studied granitic rocks can be identified using the following relations:

The AFM ternary discriminated diagram, (Fig.5D) of [62] reveals that the studied granite samples plot in calc-alkaline field with extensional trend.

The SiO_2 vs K_2O binary discriminated diagram of [63], (Fig. 5E), revealed that the studied granites plot in the high K calc-alkaline series.

The A/NK vs. A/CNK binary diagram of [64], (Fig. 5F), clears that the studied granites clear metaluminous to slightly peraluminus character.

Granitic rocks can be divided as common I-type, S-type, or A-type granites based on the source rock that melted to form the granitic magma [65]. I- type and S-type granites are derived from melts associated with orogenic processes and indicate to magma generated from meta-igneous and meta-sedimentary rocks, respectively. A-type (anorogenic) granites are not associated with orogenic processes but result from emplacement within continental crust through non-orogenic processes.

[66] designed a series of diagrams to discriminate between A-type granites, and other granitic types. On the K_2O/MgO, $(Na_2O+K_2O)/CaO$,Y and Zr versus 10000*Ga/Al diagrams (Figs. 6 A,B,C&D), the studied syenogranite samples plot in the A-type granite field.

[67] concluded that the A-type granites could be divided into two chemical groups. The first group (A_1) is characterized by element ratios similar to those observed for oceanic-island basalts. The second group (A_2) is characterized by ratios that vary from those observed for continental crust to those observed for island-arc basalts. It is proposed that these two types have very different sources and tectonic settings. The A_1 group represents differentiates of magmas derived from sources like those of oceanic-island basalts but emplaced in continental rifts or during intra-plate magmatism. The A_2 group represents magmas derived from continental crust or under-plated crust that has been subjected to a cycle of continent- continent collision or island-arc magmatism.

Also, the proposed ternary diagram $(Na_2O + K_2O)–Fe_2O_3^*\times5–$ (CaO + MgO)×5, of [68], (Fig.6E), based on the molecular quantities of rock-forming oxides, permits the reliable separation of *A*-type granitoids and felsic igneous rocks of other types.

recognized fields of *A*-type rocks correspond to two petrogenetic types: resulted from the differentiation of alkali-basaltic magmas with minor assimilation (*A*1)

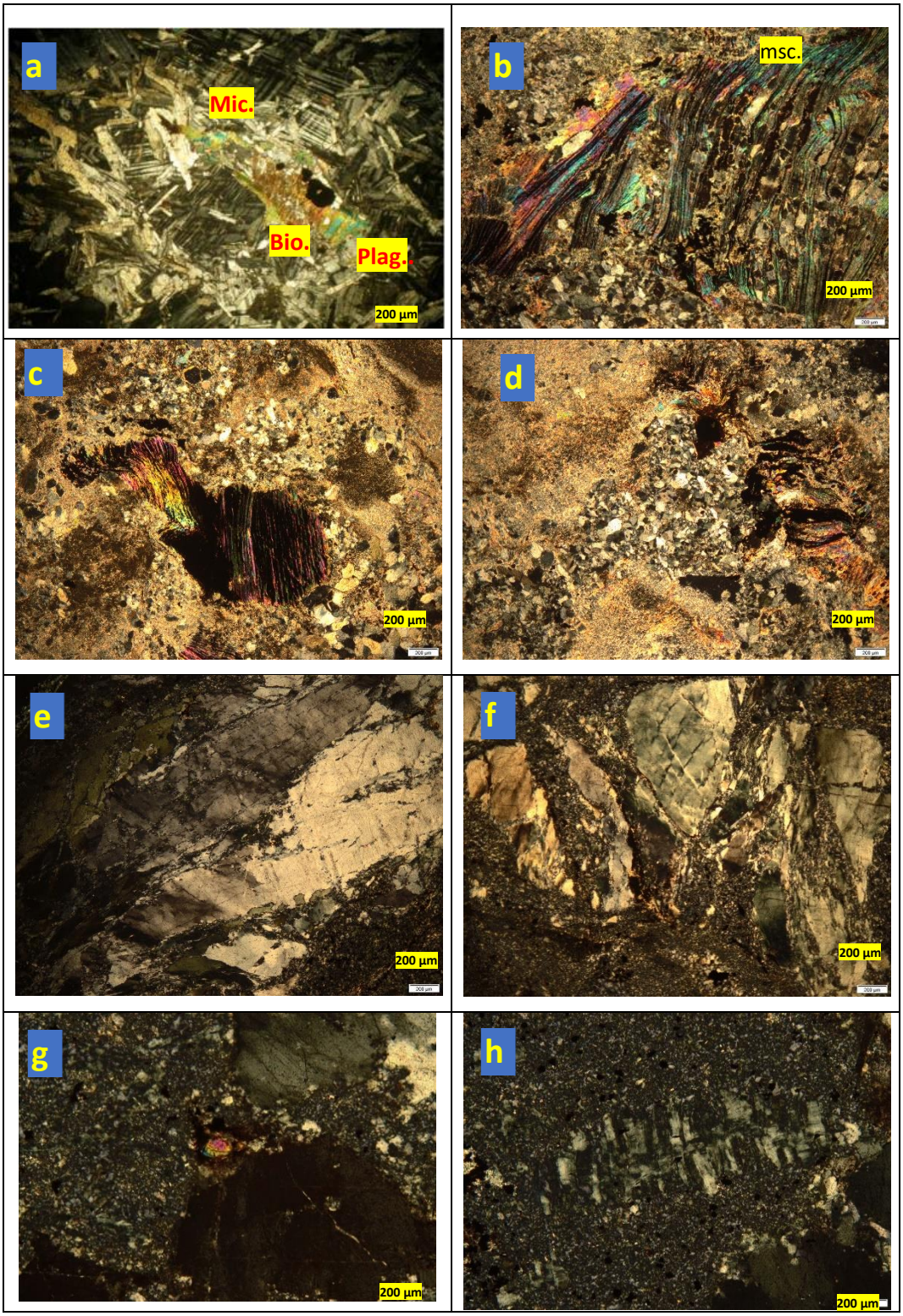

Fig. 3:
a.. Euhedral microcline, microcline (Mic.) perthite and plagioclase (Plag.) crystals associated with biotite flakes (Bio.) that altered to muscovite and chlorite C.N.
b.. kinked muscovitized (msc.) biotite flakes with skeletal reworked silica as a result of shearing and silicification C.N.
c. replacement of iron along cleavage planes as a result of hematization with hydrothermal solutions C.N.
d. Reworked silica as a thermal effect of hydrothermal solutions C.N.
e. Undulose extinction of quartz (qz.) as a result of shearing and reworking of hydrothermal solution. C.N.
f. Mylonitization (brecciation) of quartz as a result of sheairng with increasing silicification. C.N.
g.Amorphous radioactive mineral associating zircon embedded within fine grained silica groundmass. C.N.
h. Remnant of microcline crystal due to intensive silicification C.N.

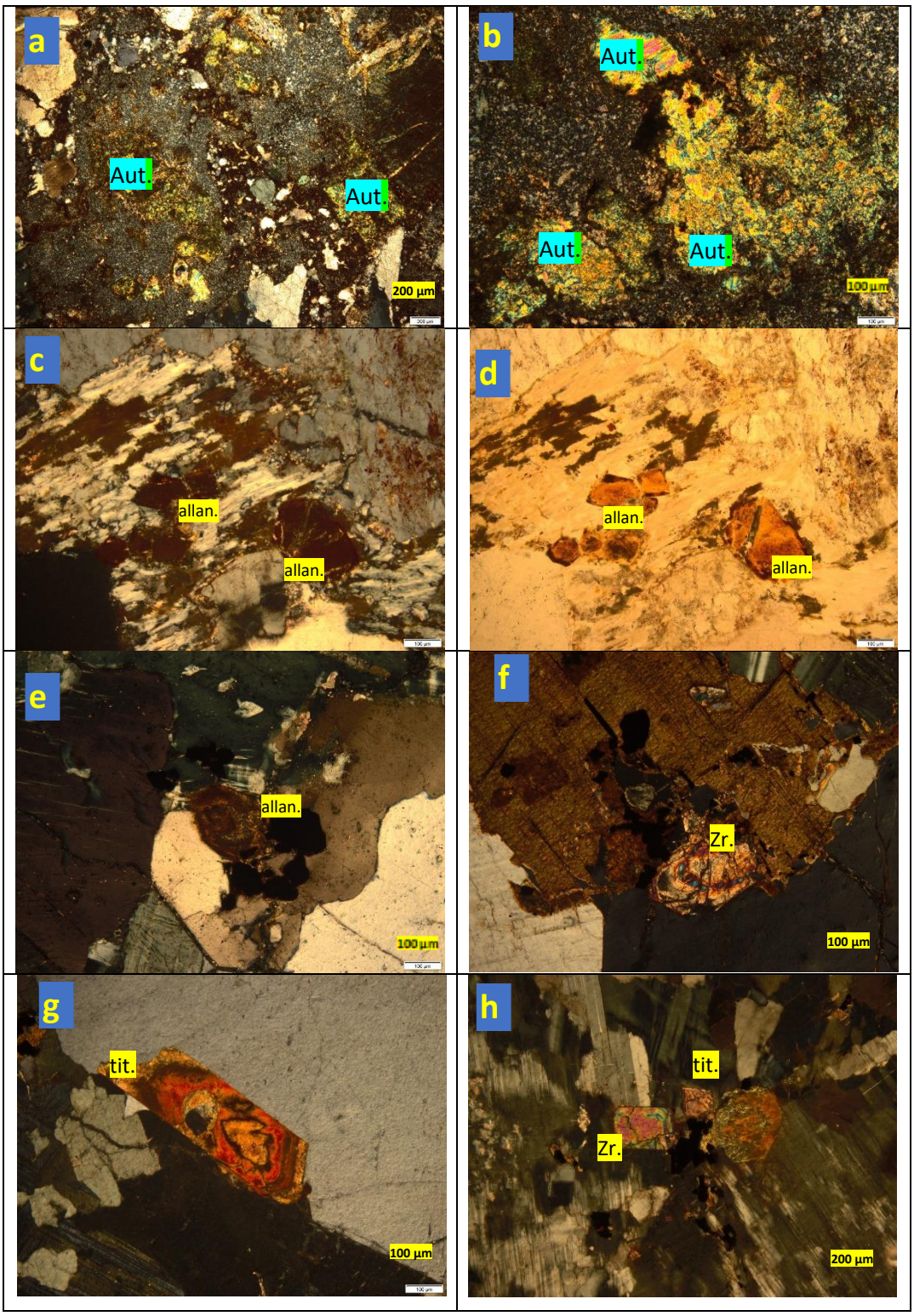

Fig.4:
a. Batches filled with autonite (Aut.) within hydrothermally altered Erediya monzogranite
b. Autonite dehydrate to meta autonite, C.N.
c, d. Euhedral crystal of allanite under crossed nicols and plane polarized light.
e. Zoned allanite (allan.) crystal engulfed within quartz crystal associating microcline perthite
f. Two subhedral zoned metamict zircon crystals associating biotite flakes.C.N
g. Euhedral zoned titanite (tit.) crystal with opaque inclusions engulfed within coarse quartz crystal.
h. Swelling and fracturing of zircon crystal due to metamictaization associating titanite within plagioclase laths.

Table 1: Major oxides, trace elements, Rare earth elements and CIPW norm, for the studied granites.

sample	1	2	3	4	5	6	7	8	9	10	11	12	13	14	15	16
SiO_2	75.5	77.5	77.6	76.7	74.7	75.5	76.5	74.4	75.9	76.8	75.8	74.6	74.8	74.8	75.1	75.3
TiO_2	0.2	0.1	0.1	0.1	0.1	0.1	0.1	0.1	0.1	0.1	0.1	0.2	0.2	0.1	0.1	0.1
Al_2O3	12.5	12.4	12.0	12.6	12.8	12.0	12.2	13.2	12.4	12.5	12.1	11.9	11.9	12.2	12.3	12.3
Fe_2O_3	1.6	0.6	1.0	1.1	1.4	1.2	0.9	1.1	1.2	1.0	1.7	1.2	1.2	1.0	1.4	1.3
MnO	0.0	0.0	0.1	0.1	0.0	0.0	0.1	0.1	0.0	0.0	0.1	0.0	0.0	0.1	0.1	0.1
MgO	0.1	0.0	0.0	0.0	0.1	0.0	0.0	0.0	0.0	0.0	0.0	0.1	0.1	0.1	0.0	0.1
CaO	0.8	0.2	0.5	0.3	0.6	0.6	0.5	0.7	0.5	0.4	0.5	0.5	0.4	0.5	0.7	0.6
Na_2O	3.8	4.0	4.0	3.7	4.9	3.7	3.8	4.1	3.8	3.2	3.7	3.9	4.0	4.0	4.1	4.1
K_2O	4.4	4.4	4.4	5.1	4.1	5.1	4.8	5.0	5.1	4.8	4.7	4.7	4.5	4.9	4.8	4.6
H_2O^+	0.5	0.5	0.8	0.7	0.6	0.5	0.5	0.8	0.7	0.6	0.7	0.5	0.5	0.8	0.7	0.6
CO_2	0.1	0.1	0.1	0.1	0.0	0.1	0.1	0.1	0.1	0.0	0.1	0.1	0.1	0.1	0.1	0.0
Total	99.6	99.9	100.5	100.4	99.4	98.9	99.5	99.6	99.8	99.6	99.4	97.7	97.8	98.6	99.6	99.1
Rb	155.0	172.0	152.0	162.0	212.0	161.0	182.0	198.0	172.0	151.0	135.0	200.0	215.0	285.0	295.0	251.0
Ba	241.0	139.0	87.0	71.0	69.0	175.0	89.0	294.0	125.0	103.0	270.0	85.0	130.0	190.0	100.0	105.0
Sr	70.0	80.0	85.0	72.0	74.0	69.0	75.0	69.0	66.0	78.0	69.0	66.0	72.0	59.0	69.0	57.0
Zr	137.0	92.0	98.0	97.0	108.0	120.0	85.0	173.0	112.0	119.0	163.0	196.0	180.0	172.0	187.0	200.0
Hf	7.7	8.3	6.9	6.0	7.7	6.4	7.2	5.5	7.3	5.8	6.4	6.4	7.6	6.1	7.3	7.8
Nb	76.0	83.0	85.0	79.0	74.0	72.0	70.0	68.0	70.0	75.0	73.0	74.0	81.0	77.0	81.0	78.0
Ta	5.0	6.0	7.0	6.5	4.5	4.0	5.8	3.5	4.2	4.5	4.2	3.6	3.6	3.9	4.3	4.7
Ga	26.0	30.0	32.0	28.0	26.0	30.0	34.0	29.0	31.0	35.0	32.0	27.0	26.0	27.0	29.0	30.0
Y	72.0	82.0	85.0	70.0	63.0	64.0	69.0	62.0	70.0	64.0	68.0	66.0	68.0	66.0	75.0	80.0
U	17.0	19.0	22.0	17.0	18.0	14.0	16.0	15.0	19.0	22.0	20.0	14.0	15.0	15.0	16.0	18.0
Th	68.0	76.0	72.0	60.0	62.0	51.0	57.0	52.0	58.0	65.0	60.0	38.0	40.0	48.0	57.0	55.0
La	11.0	12.0	17.0	13.0	15.0	19.0	14.0	18.0	14.0	17.0	22.0	11.0	20.0	12.5	13.0	16.0
Ce	63.0	55.0	71.0	69.0	87.0	73.0	58.0	64.0	77.0	83.0	68.0	60.0	66.0	58.0	54.0	69.0
Nd	33.0	45.0	47.0	31.0	34.0	51.0	46.0	38.0	31.0	44.0	55.0	41.0	48.0	36.0	33.0	39.0
Sm	4.7	4.0	5.0	3.9	3.5	4.6	3.2	4.7	4.2	3.6	4.1	3.2	2.8	4.0	3.9	2.7
Eu	0.3	0.5	0.4	0.4	0.5	0.4	0.4	0.4	0.5	0.4	0.4	0.4	0.5	0.5	0.4	0.5
Gd	4.7	6.0	5.3	4.9	5.0	6.3	5.8	4.7	4.4	5.2	6.3	4.1	4.9	4.7	5.7	6.8
Tb	1.0	1.3	1.2	1.1	0.9	0.9	1.2	1.3	1.0	0.9	1.2	1.0	0.9	1.2	0.9	1.4
Yb	12.4	13.2	11.9	12.7	13.0	12.3	11.9	10.9	13.6	11.6	13.4	11.9	12.7	12.5	11.6	13.8
Lu	1.8	2.2	1.6	2.3	1.8	1.5	2.1	1.9	2.6	2.4	1.8	1.6	1.8	2.0	2.2	2.0
Q	34.8	37.3	36.8	35.4	29.8	34.0	35.1	30.3	33.6	39.1	35.7	33.7	34.1	32.3	32.7	33.9
Ab	32.2	33.8	33.8	31.3	41.1	30.8	32.4	34.4	31.9	27.1	31.1	33.1	33.9	34.2	34.8	34.4
Or	26.1	26.1	26.1	30.0	24.4	29.8	28.5	29.6	30.1	28.5	27.8	28.0	26.7	29.1	28.4	27.2
La/Yb	0.887	0.909	1.429	1.024	1.154	1.545	1.176	1.651	1.029	1.466	1.642	0.924	1.575	1.000	1.121	1.159
La/Sm	2.340	3.000	3.400	3.333	4.286	4.130	4.375	3.830	3.333	4.722	5.366	3.438	7.143	3.125	3.333	5.926

and from the interaction of mantle melts with felsic continental crustal material accompanied by serious contamination (*A*2). This diagram must be applied to interprete the geodynamic formation conditions with caution. It should be used as a tool for a comprehensive analysis of obtained geological, petrological, and geochemical information.

Nevertheless, *A*1-type rocks form mostly in the intraplate magmatism setting: in intraoceanic system (oceanic islands) or near the divergent boundaries of lithospheric plates in cold intracontinental rifts, whereas *A*2-type rocks are generated in the post collisional (or late-collision) setting as well as during the lithospheric-plate sliding and at the late stages of evolution of hot rift structures.

All of the studied granite samples plot in (A2) field, except one sample.From the previous diagrams, we can conclude that, the studied granites are true granites in composition and characteristics and most probably originated from high K calc-alkaline magma. The studied granites predominantly show metaluminous to slightly peraluminous nature and syenogranites are A2-type granites.

5.b Tectonic Setting and Source Rocks

[70] classified granites according to their intrusive settings into four main groups; Ocean Ridge Granites (ORG), Volcanic Arc Granites (VAG), Collision Granites (COLG) and Within Plate Granites (WPG). Furthermore, the

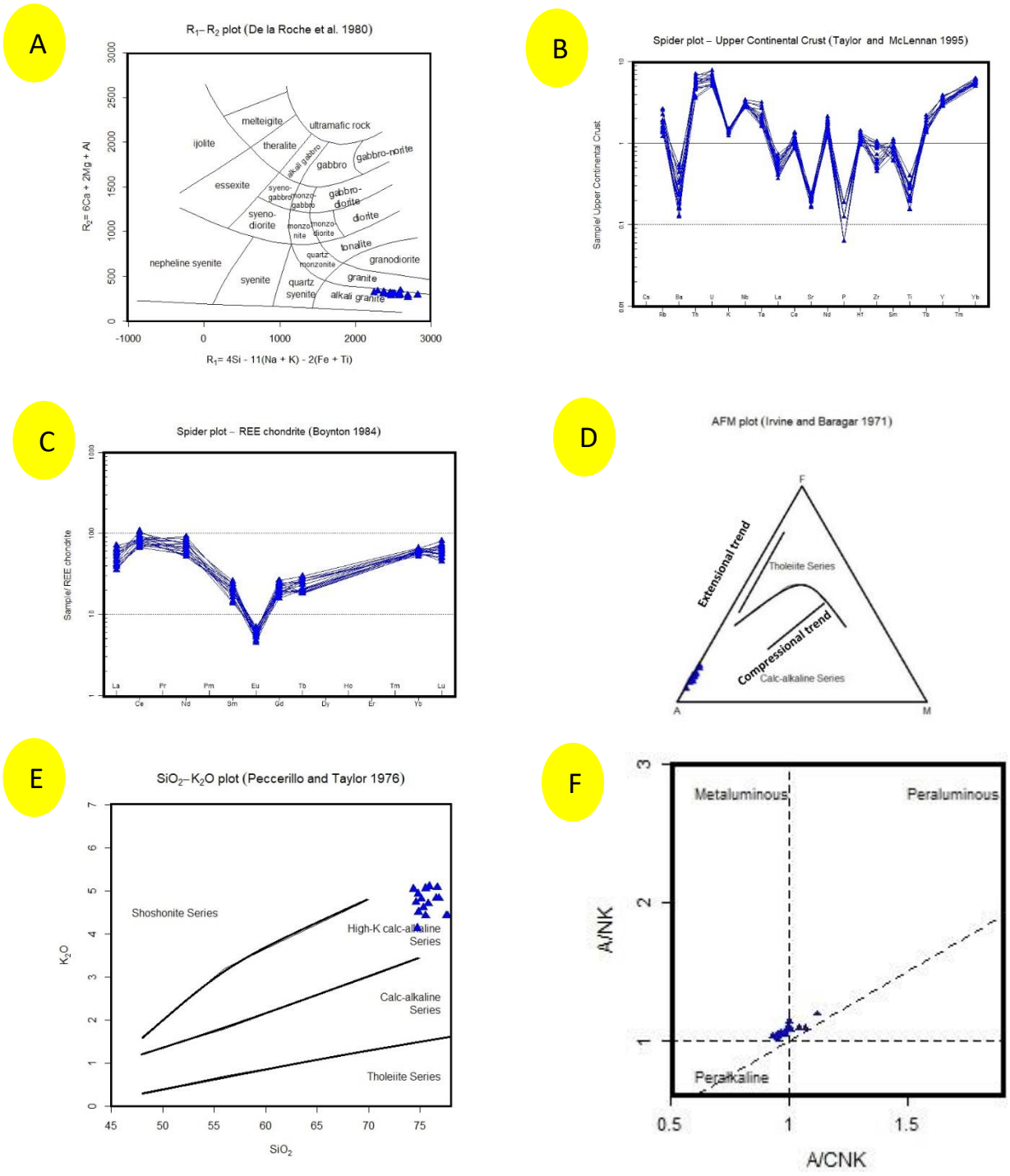

Fig. 5A: R_1 vs. R_2 classification diagram (De La Roche et al., 1980) for the studied granites. Fig. 5B: Multi-element distribution diagrams for the studied granites. Normalization values after Taylor and McLennan, 1995. Fig. 5C: Chondrite normalized REE patterns for the studied granites. Normalization values after [69]Fig. 5D: AFM ternary diagram after Irivine and Baragar, (1971) for the studied granites. Fig.5E: The SiO_2 vs K_2O binary diagram after (Peccerillo and Taylor, 1976) for the studied granites. Fig. 5F: A/NK vs. A/CNK binary diagram after (Maniar & Piccoli, 1989) for the studied granites.

granites within each group may be subdivided according to their petrological characteristics. Therefore, a direct genetic relationship between chemical composition of granites and their tectonic setting has been established (e.g. [70-72]; etc.....). The tectonic setting of the younger granites could be deduced from many discrimination diagrams which are constructed from major oxides, trace elements and their inter relations.

In the R_1-R_2 binary diagram (Fig. 7A) of [73] the syenogranite samples fall in the Post orogenic field. [70] stated that volcanic arc granites (VAG) can vary in setting from oceanic to continental and in composition from tholeiitic through calc-alkaline to shoshonitic. They defined collisional granites as syn- or post-tectonic granites associated with continent continent collision, or syn-tectonic granites associated with continent arc collision. On the Nb (ppm) versus Y (ppm) and Rb (ppm) versus Y+Nb (ppm) discrimination diagrams of [70] (Figs. 7B,C) the syenogranites plot in the within plate granites field (WPG).

Several source rocks have been assumed to elucidate the generation of granitic magmas by partial melting mechanism. Partial melting under variable conditions of various source rocks output granitic melts of different composition. The source rocks from which the granitoids were generated can be deduced through the following relationships:-

The variations between the Al_2O_3 / (FeOt+ MgO), 3*CaO , 5*(K_2O / Na_2O), on the ternary discrimination diagram of [74] shows that the studied syenogranite rock samples are derived from tonalite rocks or crustal sources (Fig. 7D).

5.c Magma Conditions

The CIPW normative compositions are more useful tools in giving some information about the P-T conditions of granitic magma crystallization. On the Ab- The CIPW normative compositions are more useful tools in giving some information about the P-T conditions of granitic magma crystallization.

On the Ab-Q-Or ternary diagram (Fig. 7E) of [75], the studied granites are clustered around the isobaric univariant curve in water vapor between 2-5 Kbar [76]. The investigated granites lie in the granite field and are clustered around the isobaric curve, >1 -5 kb P_{H2O}. water vapor pressure, (Winkler et al., 1975) suggesting crystallization at moderate depth and the crystal-liquid equilibrium was the dominant mechanism involved in the genesis of these granites.

Using the thermal lines on the Ab-Q-Or ternary diagram, According to [77], the estimated temperatures are about 820-840ºC for the studied syenogranites (Fig. 7F).

A binary relation between Rb (ppm) and Sr (ppm) was suggested by [78] to estimate the crustal thickness. The studied syenogranites have been generated at greater depth >30 km of the lower crust (Fig. 7G).

5.d Geochemical Characteristics of the Altered Granites.

Eleven samples from EI-Erediya altered granite samples were selected and prepared for geochemical analysis of major oxides, trace elements and **CIPW** Norm values as shown in Table 2. According to the normative Qz-Ab-Or composition, the altered rock samples could be classified into sodic, potassic, silicic and greisen (Fig. 7H). The studied altered granites samples have high SiO_2 content and shifted towards quartz, also show imprints of silicfication with some tendency towards greizenization as indicated by [79]. The ternary minimum for 1 kb H_2O pressure from [80] and the stars represent the ternary minima for a granite system with 0% and 4% F [79]. They plot above the granitic eutectic temperature and exhibit a trend corresponding to crystallization in higher P_{H2O} range; [81]. The trends of granitic alteration types are from [55].

The Na% vs. K% variations diagram afer Cuney et al. (1989) shows five trends; Na-metasomatism, K-metasomatism, silicifcation, desilicifcation and argillation trend (Fig. 7I). Most of the studied altered granite samples lie in silicification, desilicification, K-metasomatism, and argillation trend. According to [82], plotting on AKF ternary diagram (Fig. 7J), where A= Al_2O_3 - (Na_2O + K_2O), K= K_2O and F= FeO + MnO + MgO. It shows that only four samples of the altered granites fall in sericite facies (due to sericitization processes, containing plagioclases and K-feldspars, both of which were converted to sericite) and the other samples fall in propylitic feld (containing epidote and chlorite alteration).

On the (Na_2O+CaO) – MgO+Fe_2O_3 binary diagram [83] altered granite samples include substantial variations in the concentrations of Na, Ca, Mg and Fe (Fig. 7 K) . Increasing alteration intensity is coupled with a gradual decrease in Na_2O and CaO, culminating in intensely altered samples having lower Na_2O+CaO values wt%. This trend is indicative of plagioclase destruction and formation of muscovite/sericitization. We can conclude that the hydrothermal alterations are common in the form of silicification, hematitization, sericitization , greisenization and kaolinitization.

6 Radioactivities

6.1 Distribution of Uranium and Thorium in El Erdieya Syenogranites

A total number of 15 samples representing the studied granites were analyzed to determine eU, and eTh contents for the fresh granites as well as 15 samples representing eU and eTh for the mineralized samples, as shown in Table 3. The comparison of granites and altered varieties of the

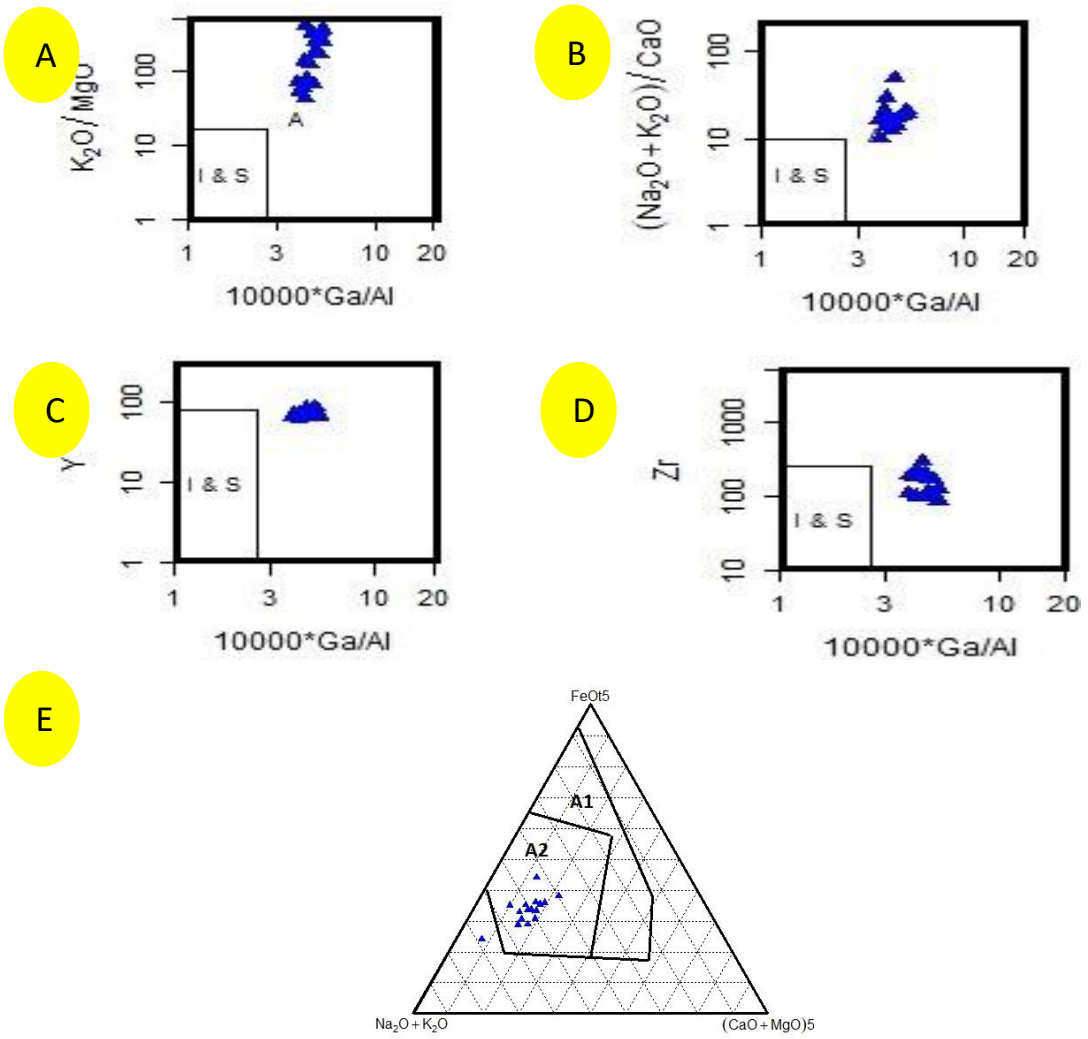

Fig. 6 : Discrimination diagrams after Whalen et al., (1987) for the studied granites; (a) 10000*Ga/Al versus K_2O/MgO, (b) 10000*Ga/Al versus $(Na_2O+K_2O)/CaO$, (C) 10000*Ga/Al versus Y and (D) 10000*Ga/Al versus Zr. (E**)** Na_2O+K_2O-FeOt*5-(Cao+MgO)*5 ternary diagram after (Grebennikov, 2014) for the studied syenogranites.

Table 2: Major oxides, trace elements, and CIPW norm, for the studied altered granite samples.

	serecitized granite			hematized granite				jasperoid veins			
sample	**Er-6**	**Er-7**	**Er-8**	**Er-9**	**Er-10**	**Er-11**	**Er-12**	**Er-13**	**Er-14**	**Er-15**	**Er-16**
SiO_2	76.1	75.3	76.15	79.3	79.2	78.8	76.1	89.1	87.64	88.2	89.1
TiO_2	0.1	0.09	0.08	0.02	0.01	0.03	0.02	0.01	0.03	0.04	0.05
Al_2O3	8.7	9.2	7.8	13.84	11.4	11.8	11.26	6.3	5.22	4.15	3.41
Fe_2O_3	4.63	4.9	4.5	5.91	7.4	4.93	5.87	2.17	2.1	2.02	1.33
MnO	0.1	0.06	0.08	0.05	0.02	0.04	0.01	0.03	0.04	0.02	0.01
MgO	0.06	0.05	0.04	0.12	0.04	0.08	0.03	0.03	0.02	0.02	0.01
CaO	0.53	0.5	0.41	0.2	0.14	0.15	0.08	0.04	0.06	0.03	0.03
Na_2O	2.61	1.72	2.65	1.15	0.06	1.12	1.08	1.06	0.087	0.083	0.07
K_2O	3.58	3.33	3.3	4.32	4.2	3.24	3.52	1.81	1.7	1.35	1.4

P_2O_5	0.013	0.012	0.015	0.02	0.01	0.02	0.01	0.01	0.01	0.01	0.01
H_2O^+	4.1	1.98	1.3	1.6	1.2	1.4	0.9	1.3	0.85	1.1	1.25
CO_2	0.21	0.31	0.18	0.3	0.28	0.32	0.22	0.5	0.4	0.2	0.1
Total	100.73	97.45	96.51	106.83	103.96	101.93	99.10	102.36	98.16	97.22	96.77
Ba	150	125	100	310	148	164	105	470	280	205	150
Ga	29	23	23	34	28	32	22	20	19.6	17.4	15
Hf	8	5.9	5	7.6	5.2	4.8	4.3	6.1	5.1	4.2	2
Nb	74	58	48	101	64	74	h	125	99	105	41
Rb	145	128	90	153	87	124	69	16	15	13	12
Sr	34	27	25	83	62	56	31	106	94	96	75
Ta	5.2	4.1	2.8	7.2	4.3	3.8	3.1	8	6.8	8.6	2.6
Zr	300	230	180	275	246	162	159	230	204	158	79
Y	90	72	48	68	42	58	38	100	74	59	26
Pb	49	35	30	26	22	24	16	360	268	245	106
U	41	35	23	30	26	32	23	1850	490	369	320
Th	40	36	26	40	38	39	19	26	21	18	15
Q	47.13	52.49	60.51	55.88	62.72	65.58	62.13	81.66	80.60	82.53	79.33
Ab	22.09	14.55	5.50	9.73	0.51	1.02	0.68	0.68	0.74	0.70	0.59
Or	21.16	19.68	13.59	25.53	24.82	19.15	20.80	10.70	10.05	7.98	8.27
K%	2.97	2.76	1.91	3.59	3.49	2.69	2.92	1.50	1.41	1.12	1.16
Na%	1.94	1.28	0.48	0.85	0.04	0.09	0.06	0.06	0.06	0.06	0.05

studied area with the reported ranges and averages of [84]; [85]; [86]; [87]; [88] and [89] shows that the studied syenogranites have some enrichment of uranium relative to the normal contents of uranium and thorium. So, the studied syenogranites can be considered as a uraniferous granites (with high U and Th contents), whereas the mineralized samples along the shear zone exhibit the most anomalies targets, especially in the red and black silica. These silica veins are considered as fertile rocks, therefore, it is logically that they took a great attention in radioactive survey of the study area.

6.2 Variation Diagrams of Uranium and Thorium in the Studied Granitoids

A number of variation diagrams have been used to provide useful information about the relation between eU, eTh, and eTh/eU within both the fresh and mineralized samples . These variation diagrams (Fig.8) will be discussed in the following paragraphs.

The relation between uranium and thorium may indicate the enrichment/or depletion of uranium and/or thorium. The eU-eTh scatter diagram of the studied granite samples (Fig.8A, B), shows that the majority of samples have a strong direct relation with U enrichment in mineralized samples. The relation between eTh and eTh/eU (Fig.8C, D) exhibits visual decreasing trends. The eTh contents also exhibit large scatter in the mineralized than the fresh samples . The scatter of the majority of the normal syenogranite samples plots as well as the mineralized samples indicate redistribution of eU by the post-magmatic processes. Normally, Th is three times as abundant as uranium in natural rocks, [90]. When this ratio is disturbed; it indicates the depletion or enrichment of eU. This is very evident in the analyzed samples (Fig.8D), where the decrease in the eTh/eU ratio is accompanied by enrichment in uranium.

The curved decreasing relationships between eTh/eU ratios and eU (Fig.8E,F.) might suggest that the distribution of eTh and eU was mainly controlled by magmatic fluids. U and Th contents of granitic rocks generally increase during differentiation although in some cases they decrease [91]. eTh/eU ratio can either increase Whitfield, Rogers [92]; or decrease Larsen E.S. and Gottfried [93] as it is controlled by the redox conditions, volatile contents, or alteration by endogens or supergene solutions [94]. A clear U enrichment in (Fig.8F) in mineralized samples.

The equation eU-(eTh/3.5) indicates uranium mobilization (Fig. 8G). If the result of this equation is equal to zero, it indicates absent or at least very restricted uranium mobilization. When it is greater than zero, it means that the uranium was enriched, so the majority of the studied samples exihibit enrichment above the line (1.0). The

negative values mean uranium was leached out. However, uranium redistribution processes may also result from U mobility, during surface chemical weathering, and or mobility, during hydrothermal activity associated with the emplacement of the intrusion. The studied granites show maximum enrichment of eU contents (6501ppm) for mineralized granites. The maximum eTh content is (68 ppm) in the seyanogranites that result in uneven distribution of radioactive anomalies.

6.3 Geochemistry of Uranium and Thorium of the Studied Syenogranites

A number of variation diagrams have been used to provide useful information about the relation between U, Th and some incompatible elements within the investigated granitic rocks. These variation diagrams will be discussed in the following paragraphs.

It is well known that U, Th, Y, Zr, Rb and Nb behave incompatibly in granitic melts so that if magmatic processes controlled uranium concentration, these elements would be expected to increase. This is clearly evidenced from the U versus Ba, Y, Zr, and Nb relationships (Fig.9 A,B,Cand D), which shows positive correlation with Zr, Nb and Y indicating that the U content tends to increase with increasing contents of such elements during the magmatic processes. While negative correlation with Ba indicating uranium, enrichment is thought to be of magmatic origin.

From the previous relationships and discussions, it is clear that the studied granites could be classified as uraniferous granites. In spite of the high average equivalent uranium content of these varieties, no primary uranium minerals have been so far detected and this may suggest the existence of uranium and thorium in accessory (uranophane, autonite, monazite, zircon and xenotime) and secondary minerals as will discussed in detail later.

However, it is suggested that several processes, such as metamictization and tectonic-crushing act during and/or post-magmatic stages make it easy for hydrothermal solutions to leach uranium out of primary uranium minerals that disseminated in these rocks, or that adsorbed onto the Fe-oxides and hydroxides.

Table 3: eU and eTh of the studied Fresh and mineralized samples.

		Radiometric measurements					
	Fresh samples			Mineralized samples			
Sample No.	eU (ppm)	eTh (ppm)	eTh/eU	**Sample No.**	eU (ppm)	eTh (ppm)	eTh/eU
1	22	65	2.95	40	194	27	0.14
2	20	64	3.20	41	931	222	0.24
3	16	56	3.50	42	1185	176	0.15
4	17	58	3.41	43	156	77	0.49
5	15	47	3.13	44	43	20	0.47
6	18	61	3.39	45	316	27	0.09
7	23	68	2.96	46	235	24	0.10
8	18	50	2.78	47	138	20	0.14
9	30	55	1.83	48	91	21	0.23
10	29	79	2.72	49	354	24	0.07
11	16	43	2.69	50	4041	304	0.08
12	7	20	2.86	51	2401	305	0.13
13	5	17	3.40	52	6501	50	0.01
14	3	10	3.33	53	50	17	0.34
15	6	18	3.00	54	261	9	0.03

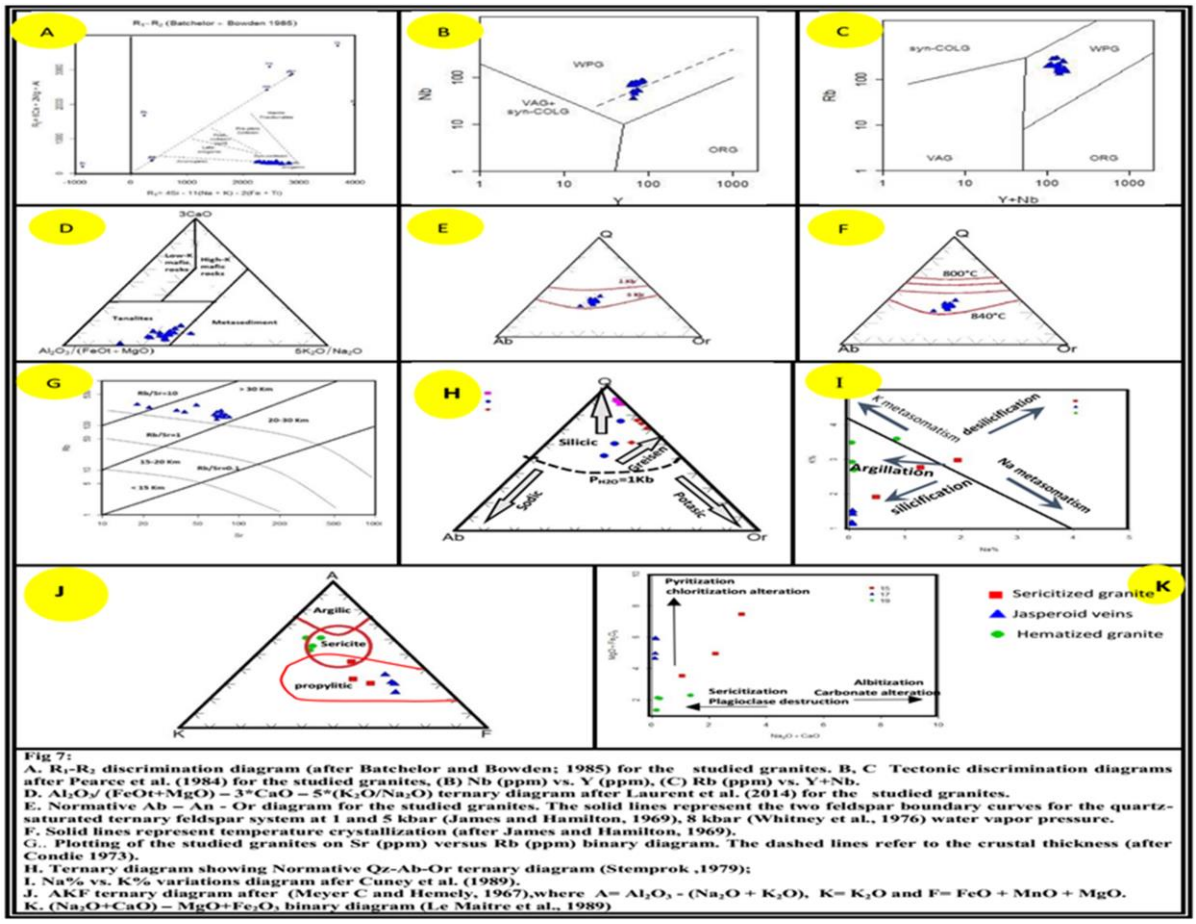

Fig 7:
A. R_1-R_2 discrimination diagram (after Batchelor and Bowden; 1985) for the studied granites. B, C Tectonic discrimination diagrams after Pearce et al. (1984) for the studied granites, (B) Nb (ppm) vs. Y (ppm), (C) Rb (ppm) vs. Y+Nb.
D. Al_2O_3/ (FeOt+MgO) – 3*CaO – 5*(K_2O/Na_2O) ternary diagram after Laurent et al. (2014) for the studied granites.
E. Normative Ab – An - Or diagram for the studied granites. The solid lines represent the two feldspar boundary curves for the quartz-saturated ternary feldspar system at 1 and 5 kbar (James and Hamilton, 1969), 8 kbar (Whitney et al., 1976) water vapor pressure.
F. Solid lines represent temperature crystallization (after James and Hamilton, 1969).
G.. Plotting of the studied granites on Sr (ppm) versus Rb (ppm) binary diagram. The dashed lines refer to the crustal thickness (after Condie 1973).
H. Ternary diagram showing Normative Qz-Ab-Or ternary diagram (Stemprok ,1979);
I. Na% vs. K% variations diagram afer Cuney et al. (1989).
J. AKF ternary diagram after (Meyer C and Hemely, 1967),where A= Al_2O_3 - (Na_2O + K_2O), K= K_2O and F= FeO + MnO + MgO.
K. (Na_2O+CaO) – MgO+Fe_2O_3, binary diagram (Le Maitre et al., 1989)

7 Mineralogy

This part deals with the mineralogical characteristics of the identified the most important radioactive and rare earth containing minerals. The detailed study revealed the presence of the following uranium and thorium minerals as well as some radioactive bearing minerals.

Uranophane Ca (UO2)2Si2O7·6H2O

Mineralized rock samples are coated and stained with noticeable concentrations of secondary uranium minerals. The most common secondary uranium minerals in the studied samples are uranophane that are easily recognized by its bright lemon or canary yellow color with greasy luster. Under binocular microscope, uranophane grains separated from the studied samples are generally massive with granular form. It represents mostly as aggregates, acicular grains and thin prismatic crystals that are randomly oriented. It is an alteration product of gummite or uraninite and the chief component of the outer silicate zone of the alterations of uraninite. The hydrated oxides altered by reaction of meteoric water to form uranophane, beta-uranophane and soddyite [95] . Most uranophane appears to be of supergene origin in oxidized deposits with beta-uranophane as dimorphs [96] .[97] suggested that most of the secondary uranium minerals in the shear zones were occurred as microfractures infilling or coating on joint surfaces and formed by replacing of primary uranium-thorium minerals (uraninite, pitchblende and/or thorite) as a result of pH and/or Eh changes through the effect of hydrothermal fluids. Uranophane was identified by ESEM data (Fig. 11.A).

Uranophane Ca (UO2)2Si2O7·6H2O

Mineralized rock samples are coated and stained with noticeable concentrations of secondary uranium minerals. The most common secondary uranium minerals in the studied samples are uranophane that are easily recognized by its bright lemon or canary yellow color with greasy luster. Under binocular microscope, uranophane grains separated from

Uranothorite [(Th, U, Ce) SiO4]

The decomposition of thorite to uranothorite in an oxidizing environment and in acidic hydrothermal solutions. It suggested that the studied area was affected by hydrothermal solutions enriched in U and Th. It varies in color from dark brown, grayish yellow and deep brown to

deep yellowish green. It is interstitially associated with iron oxides. It is partially magnetic due to its low content of iron oxides. Uranothorite was identified by ESEM data (Fig. 11.B).The EDAX analysis data of examined thorite shows in the attached table.

Zircon ($ZrSiO_4$)

Zircon is a common accessory mineralin the Na-rich plutonic rocks and show variations in morphology, color, chemistry, radioactivity and source. Under the binocular microscope, the studied zircon varies from short prismatic crystals to euhedral dull edges. Most of the studied samples from G. El Erediya contain zircon as accessory minerals. [60] stated that zircon as the major source of HREE in granitic rocks, while [98] considered partitioning of HREE between zircon and apatite. [99] concluded that when zircon enclosed by biotite or other colored silicates, it sometimes gives rise to pleochroic haloes due to its content of radioactive element. . Morphologically, the crystals of this type are short or equi-dimensional displaying metamictization due to the presence of radioactivity atoms zircon crystals. Metamictization in minerals is generally considered to be the effect of radiation damage produced by radioactive decay of thorium and uranium [100]. They are transparent to translucent and their colors range from colorless to pale brown . Most of zircon mineral grains are translucent to opaque and range in color from pale yellow to dark brown color. [101] attributed the coloration of zircon in the Egyptian granitic rocks to hydrothermal solutions. Zircon was identified by ESEM analysis (Fig. 11.C).

Xenotime (YPO_4)

Xenotime is a rare earth phosphate mineral; whose major component is Ytterbium phosphate.

Xenotime occurs as an accessory mineral in El Erediya syenogranite interfiling between crystals or as inclusions. The studied xenotime crystals contain high REE (Sm, Gd, Dy, Er, Yb) contents. The crystals are cracked as a result of radioactive constituents. Xenotime is confirmed by ESEM (Fig. 11.D). [102] considered xenotime is a good host for the rare earth elements, where it concentrated the heavy rare earth. Xenotime is also confirmed by ESEM (Fig. 11.D).

Allanite (Ca, Ce, Y, La)2 (Al, Fe^{+3})3(SiO4)3(OH) ,

Allanite is the most abundant rare earth element bearing mineral of the epidote group [103]. Allanite is a common accessory mineral in many granitic rocks and pegmatites. These minerals are mainly enriched in Ce and Nd, suggesting that they mainly result from thorite dissolution. Magmatic allanite shows strong preference for light rare earth elements over heavy rare earth elements. Due to the presence of radioactive elements (U&Th), partial metamictization of allanite is a common phenomenon. Allanite may be replaced by thorite during weathering and thorium may be released from allanite and becomes concentrated in secondary phases [104]. The study allanite occurs as brown subhedral to euhedral prismatic crystals. The study allanite is associated with biotite. Analytical results by ESEM (Fig. 11.E) show that the structure of allanite is strongly selective for LREE, where cerium (Ce, La) predominates over all other HREE, and therefore the examined mineral corresponds to allanite-(Ce) [104]. Due to their similarity to the rare earth elements in ionic radius, uranium and thorium may be incorporated in the structure of allanite.

Titanite [CaTiSiO5(O, OH, F)]

Titanite is an accessory mineral in igneous rock. It occurs as aggregates of brown, yellow and colorless with resinous luster. In general, the color is correlated with iron content where the black or brown varieties contains more than 1% Fe2O3 [99] . Titanite grains appear as subhedral prismatic edge-shaped and concentrated in non-magnetic fractions from granitic rocks. (Fig. 11.F).

Apatite [Ca5(PO4, CO3, OH)]

Apatite is a group of phosphatic minerals having a wide range as accessories in igneous rock. The apatite is a very common mineral which is formed in early stages of formation in all types of igneous rocks. It usually occurs as tiny euhedral crystals associated with ferro-magnesium minerals. Apatite grains are transparent and have pale milky white color. The color of apatite is extremely variable. The intensity of the apatite color increases with an increase of Mn content [99] Apatite occurs with minor amounts in granite as flour- apatite. They are euhedral to subhedral grains, having short prismatic outlines and vitreous luster. Scanning electron microscopic data is shown in (Fig. 12.A).

Monazite (Ce, La, Nd, Th) PO4

onazite is the predominant LREE phosphate mineral with appreciable substitution of thorium for REE and Si for phosphorous [95]. Most of monazite mineral grains occur as minute isolated spherical grains. It is yellowish to reddish brown mineral with vitreous luster. The ESEM analysis of some monazite grains and mineral EDAX shows that they are characterized by high Ce, Nd contents (Fig. 12.B). [105] suggested that Th is commonly thought to enter the monazite structure with a (+4) oxidation state with Si (Th+4+Si+4→REE+3+P+5). Th-rich monazite has been suggested to be more susceptible to alteration than Th-poor accessory minerals [106]. So, Th- rich monazite in the studied samples may reflect fluid-induced alteration.

The relatively high Th content in monazite-(Ce) might suggest formation under high-temperature conditions rather than a low-temperature metamorphic event or hydrothermal alteration [107].

Autunite [Ca(UO2)(PO4)2.8-12H2O)].

Autunite is secondary uranium mineral and presents

mainly in the zone of oxidation and weathering obtained from the alteration of uraninite or other uranium-bearing veins. It is a radioactive mineral distinguished by yellow-green tetragonal plates and strong fluorescence in ultraviolet light and changes reversibly to meta-autunite on further heating to about 80◦c. The ESEM-EDX pattern of the autunite shown in (Fig. 12.C).

Columbite [(Fe,Mn)(Nb,Ta)2O6]

Columbite belongs to columbite-tantalite series where niobium is the dominant. [108] mentioned that columbite-Tantalite mineralization is spatially and genetically concerned with the post-orogenic geochemically distinct granitoids. Tantalite and columbite grade into one another, where Nb/Ta ratios are equal to 13.44. Columbite was identified by ESEM and EDX analysis (Fig. 12.D).

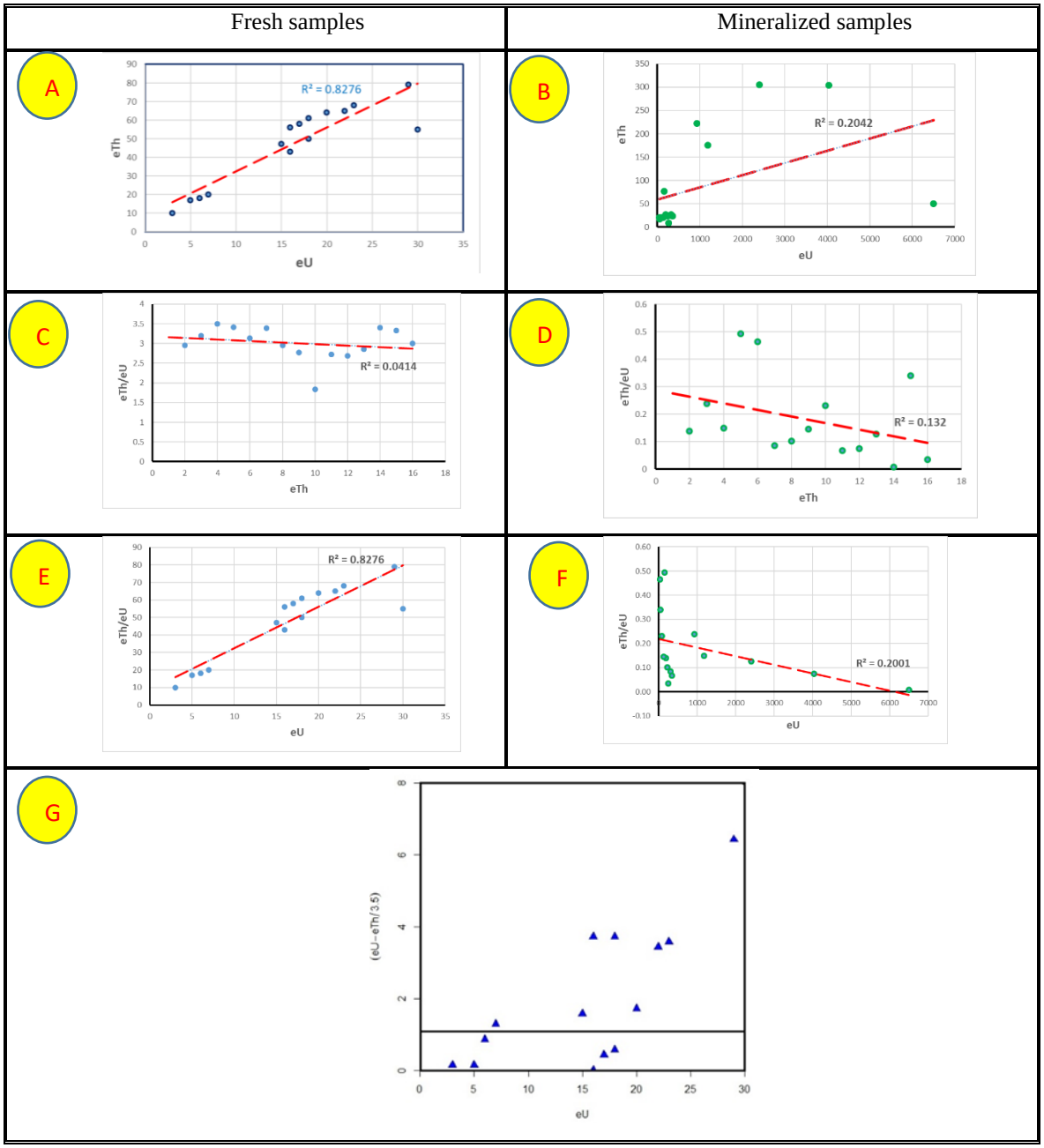

Fig.8: (A, B) eU vs. eTh, (C,D) eTh vs. eTh/eU, (E,F) eU vs. eU/eTh, (G) eU vs. (eU-eTh/3.5).

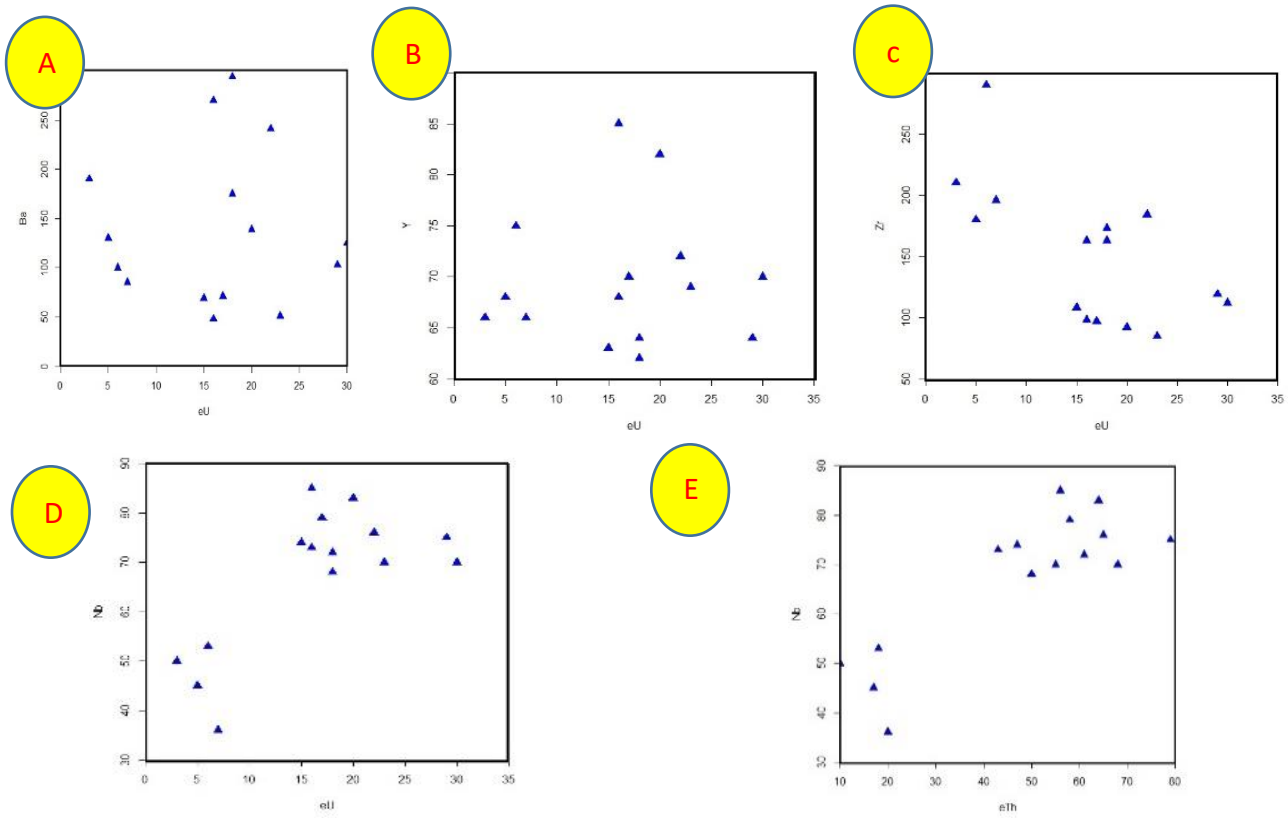

Fig.9: Variation diagrams between (A)Ba vs. eU, (B) Y vs. eU, (C) Zr vs. eU and (D) Nb vs. eU. (E) Nb vs. eTh.

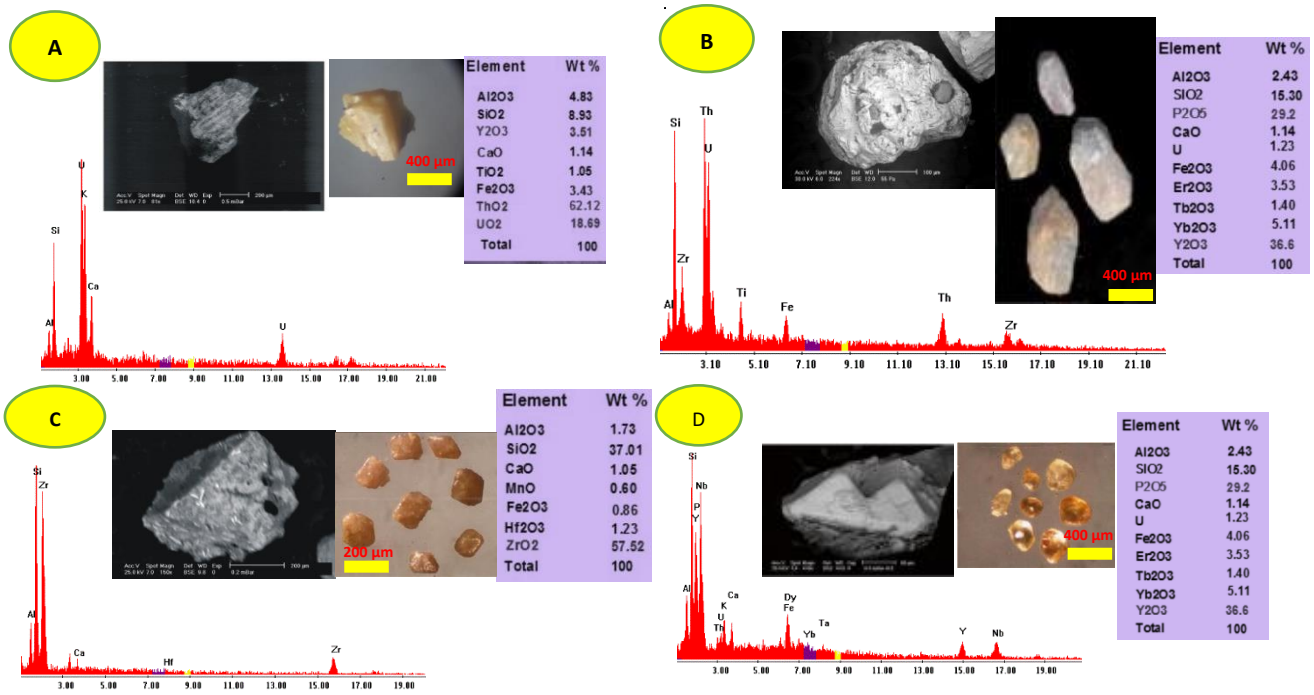

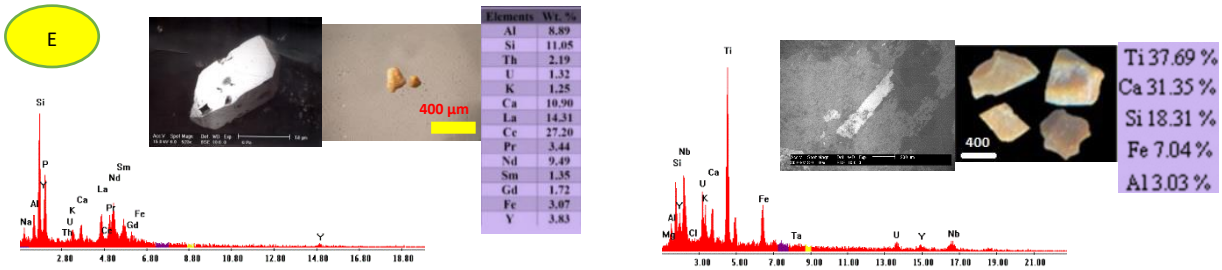

Fig. 11. EDX and BSE image showing semi-quantitative chemical composition of A) Uranophane, B) Uranothorite, C) Zircon, D) Xenotime, E) Allanite, e), F)Titanite from the studied area

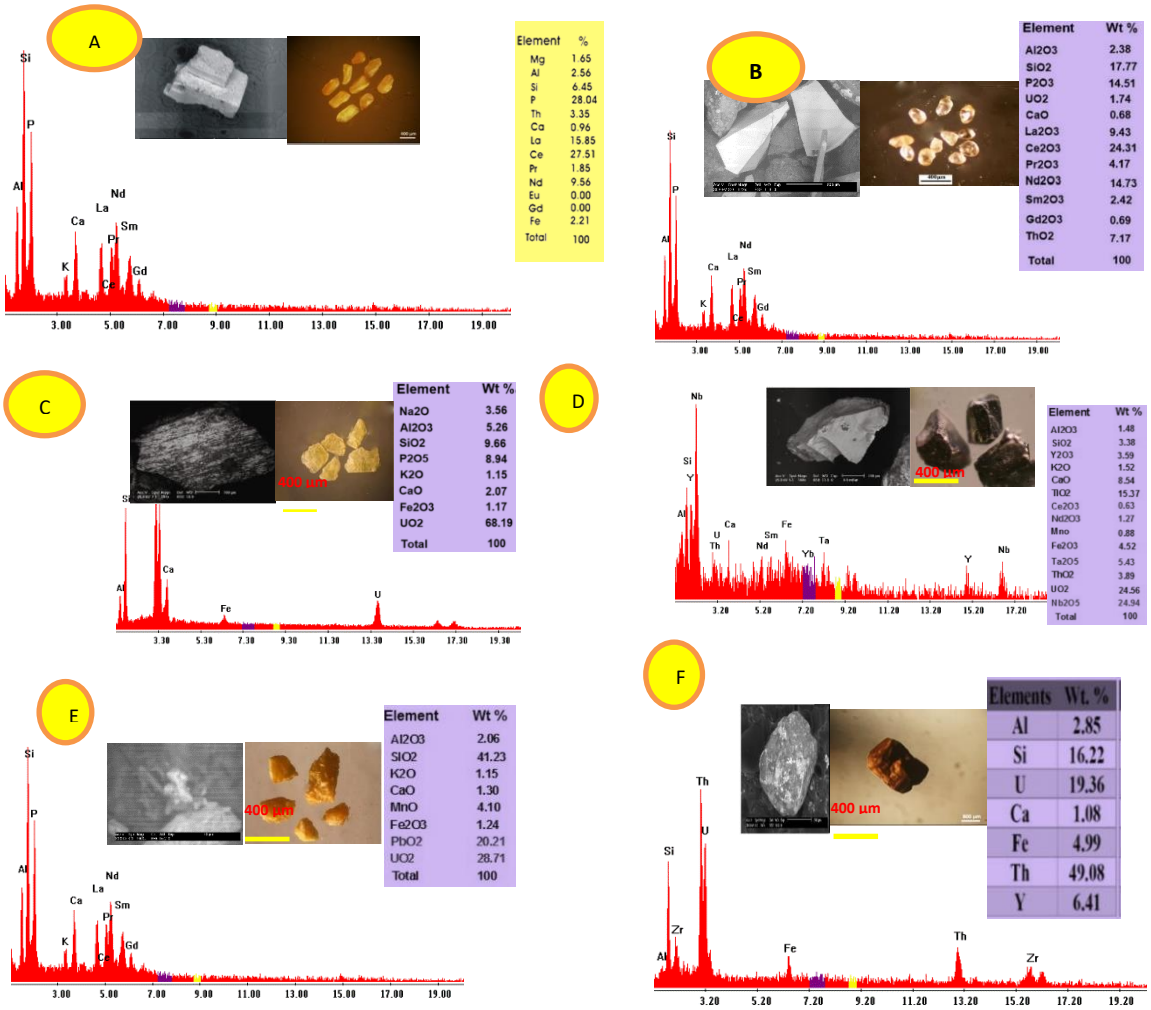

Fig. 12. EDX and BSE image showing semi-quantitative chemical composition of A)Apatite, B) Monazite, C) Autunite D) Columbite and E)Kasolite, F) Thorite.

Kasolite $Pb(UO_2)$ $SiO_4(H_2O)$.

Kasolite is the only secondary U-mineral generated by circulating meteoric water enriched in silica and Pb leached from metamict U-bearing minerals. It is characterized from the other uranium silicates by its crystal habit and luster. It is a hydrated silicate of lead and hexavalent uranium and is the only uranyl silicate with lead as its major cation. It is brightly colored (canary and lemon yellow, and brown of different intensities). The ESEM-EDX pattern of the kasolite displayed in (Fig. 12E).

Thorite [(Th SiO4)]

Thorite is a rare nesosilicate of thorium, crystallizes in the tetragonal system and is isomorphous with zircon. It is the most common mineral of thorium. Thorite forms hydrothermally (300˚ C to 700˚ C) in acidic conditions [109]. Thorite is commonly metamict and hydrated making it optically isotropic and amorphous. The color is normally black, but also brownish black, orange, yellowish orange and dark green. The studied thorite occurs as subhedral to euhedral black crystals associated with quartz, K-feldspars and biotite. Thorite is isomorphic with zircon and it is evident that a large part of thorium is incorporated in the zircon structure (Rankama and Sahama, 1955). Thorite is mainly composed as shown by EDX analysis (Fig. 12 F).

Summary and Conclusions

This work discusses the geology, geochemistry, distribution of the natural radionuclides and the mineralogical studies of the radioactive minerals in El Erediya granites, Central Eastern Desert, Egypt. G.El Erediya younger granites is located in the central Eastern Desert of Egypt, south Qena-Safaga asphaltic road, bounded between latitudes 26° 18' 36" - 26° 21' 36"N and longitudes 33° 27' 18" - 33° 30"E. This granite belongs to the post-orogenic younger granite magmatic activity that intruded the Egyptian shield between 620 and 530 Ma. EI-Erediya seyanogranites showing characteristic higher topography than the surrounding rocks. It is oval shaped, elongated in NW-SE direction and sending apophyses and offshoots within the surrounding country rocks. According to the field geological study and the previous works, the basement exposures in the area arranged from the oldest to the youngest are metavolcanics, amphibolites, younger granites, pegmatites, aplites, jaspriod veins and basic dykes. The NE trend is The main tectonic trend in the area and were rejuvenated several times causing a main faulting and fracturing followed by the injection of three phases of whites, red and black silica veins and followed by late meteoric and/or hydrothermal alterations. The common alterations are greisenization, silicification, sericitization and kaolinization,. An intense hematitization and manganese oxide staining are common along the extension of the silica veins and fractures. The red and black silica are accompanied by uranium mineralizations.

Geochemically, the studied granites are true granites in composition and characteristics and most probably originated from high K calc-alkaline magma. The studied granites predominantly show metaluminous to slightly peraluminous nature and syenogranites are A-type granites and belonging to A_2 group which represents magmas derived from continental crust or under-plated crust that has been subjected to a cycle of continent- continent collision or island-arc magmatism. The El Erediya granites were developed in within plate tectonic setting and derived from tonalite magmas or crustal sources under pressure varying between (2->5kb) and temperatures of crystallization ranging from 820^o to 840^o c, emplaced at moderate depths >30 km and the crystal fractionation was the predominant process during magmatic differentiation. We can conclude that the hydrothermal alterations are common in the form of silicification, hematitization, sericitization , greisenization and kaolinitization.

Radiometricaly, We may be concluded that the syenogranites are considered as anomalous granites and the silica veins as fertile rocks. Also, a magmatic and strong post-magmatic condition play an important role in the distribution of uranium in the studied rocks. The uranium and thorium contents are encountered in uranium and thorium minerals as well as radioactive bearing minerals such as uranophane, autonite, uranothorite, thorite, columbite, xenotime, zircon, monazite, sphene, fluorite, allanite, and apatite.

Refererences

[1] Johnson, P.R. and B.J.G.S. Woldehaimanot, London, Special Publications, Development of the Arabian-Nubian Shield: perspectives on accretion and deformation in the northern East African Orogen and the assembly of Gondwana. 2003. **206**(1): p. 289-325.

[2] Hargrove, U.S., et al., How juvenile is the Arabian-Nubian Shield? Evidence from Nd isotopes and pre-Neoproterozoic inherited zircon in the Bi'r Umq suture zone, Saudi Arabia. . Earth Planet. Sci. Lett., 2006. **252** (3–4,): p. 308–326.

[3] Vaughan, A.P. and R.J. Pankhurst, Tectonic overview of the West Gondwana margin. Gondwana Res. , 2008. . **13** (2): p. 150–162.

[4] Avigad, D. and Z. Gvirtzman, Late Neoproterozoic rise and fall of the northern Arabian-Nubian Shield: the role of lithospheric mantle delamination and subsequent thermal subsidence. . Tectonophysics 2009. **477**(3-4): p. 217–228.

[5] Stern, R.J. and P. Johnson, Continental lithosphere of the Arabian Plate: AS geologic, petrologic, and geophysical synthesis. Earth Sci. Rev. , 2010. **101** (1-2): p. 29–67.

[6] Johnson, P.R., et al., Late Cryogenian-Ediacaran history of the Arabian-Nubian Shield: a review of depositional, plutonic, structural, and tectonic events

in the closing stages of the northern East African Orogen. . J. Afr. Earth Sc., 2011. . **61**(3): p. 167–232.
[7] Fritz, H., et al., Orogen styles in the East African Orogen: a review of the Neoproterozoic to Cambrian tectonic evolution. . J. Afr. Earth Sci., 2013. **86**: p. 65-106.
[8] Garfunkel, Z., . , The relations between Gondwana and the adjacent peripheral Cadomian domain—constrains on the origin, history, and paleogeography of the peripheral domain. . Gondwana Res. , 2015. **28** (4): p. 1257–1281.
[9] Stern, R.J., . , Neoproterozoic formation and evolution of Eastern Desert continental crust - The importance of the infrastructure-superstructure transition. . J. Afr. Earth Sc., 2018. **146**: p. 15–27
[10] Fullagar, P.D., Pan-African age granites of North Eastern Africa: New or reworked sialic materials, Geology of Lybia, in Second symposium in the geology of Lybia. 1980, New York, Academic press,. p. 1050-1058.
[11] Abu Dief, A., The relation between the uranium mineralization and tectonics in some Pan-African granites, west of Safaga, Eastern Desert, Egypt, in Geol. 1992, Assiut Univ.: Assiut, Egypt. p. 218
[12] Greenberg, J.K., Characteristics and origin of Egyptian younger granites: summary. 1981. **92**(5): p. 224-232.
[13] Stern, R.J., Crustal evolution in the East African Orogen: a neodymium isotopic perspective. J. Afr. Earth Sci. , 2002. **34**: p. 109-117.
[14] Moghazi, A.M., et al., Late Neoproterozoic strongly peraluminous leucogranites, South Eastern Desert, Egypt–petrogenesis and geodynamic signifcance. . Mineral. Petrol., 2004. **81**(1-2f): p. 4r`.
[15] Farahat, E.S., et al., Origin of I-and Atype granitoids from the Eastern Desert of Egypt: implications for crustal growth in the northern Arabian-Nubian Shield. J. Afr. Earth Sc. , 2007. **49**(1-2): p. 43–58.
[16] Farahat, E.S., et al., Neoproterozoic calc-alkaline peraluminous granitoids of the Deleihimmi pluton, Central Eastern Desert, Egypt: implications for transition from late- to post-collisional tectonomagmatic evolution in the northern Arabian-Nubian Shield. . Geol. J. , 2011. **46**(6): p. 544–560.
[17] El-Bialy, M.Z. and M.M. Omar, Spatial association of Neoproterozoic continental arc Itype and post-collision A-type granitoids in the Arabian-Nubian Shield: the Wadi AlBaroud older and younger granites, north Eastern Desert, Egypt. J. Afr. Earth Sci., 2015. **103**: p. 1–29.
[18] Bentor, Y.K., The crustal evolution of the Arabo-Nubian Massif with special reference to the Sinai Peninsula. J Precambrian research, 1985. **28**(1): p. 1-74.
[19] El-Bialy, M.Z. and M.J. Streck, Late Neoproterozoic alkaline magmatismin the Arabian-Nubian Shield: the postcollisional A-type granite of Sahara-Umm Adawi pluton, Sinai, Egypt. Arab. J. Geosci. , 2009. **2**: p. 151–174.
[20] Hassan, M. and A. Hashad, Precambrian of Egypt., in Geology of Egypt., S.R. (Eds), Editor. 1990, Balkema, : Rotterdam, Netherlands. p. 201-245.
[21] El Sayed, M.M., Neoproterozoic magmatism in NW Sinai, Egypt: magma source and evolution of collision-related intracrustal anatectic leucogranite. Int. J. Earth Sci. , 2003. **92**: p. 145-164.
[22] El Shazly, S.M. and M.M. El-Sayed, Petrogenesis of the Pan-African El-Bula igneous suite, central Eastern Desert, Egypt. J. Afr. Earth Sci., 2000. **31**: p. 317-336.
[23] El Sayed, M.M., Tectonic setting and petrogenesis of the Kadabora pluton: a late Proterozoic anorogenic A-type younger granitoid in the Egyptian Shield. . Chem Erde, 1998. **58**: p. 38-63.
[24] Moghazi, A.M., et al., Geochemical and Sr–Nd–Pb isotopic data bearing on the origin of Pan-African granitoids in the Kid area, southeast Sinai, Egypt. J. Geol. Soc. London, 1998. **155**: p. 697-710.
[25] El Sayed, M.M., et al., Geochemistry and petrogenesis of the Neoproterozoic granitoids in the Central Eastern Desert, Egypt. Chem. Erde., 2002. **62**: p. 317-346.
[26] Bakhit, F.S., Geology and radioactive mineralization of Gabal ELMissikat area, Eastern Desert, Egypt. 1978, Ain Shams University: Cairo, Egypt.
[27] El-Taher, M.A., Radioactivity and mineralization of granitic rocks of El- Erediya occurrence and its comarison to El Missikat -Rea El Garra occurrence, Eastern desert, Egypt. 1985, Al Azhar Univ.: Fac. of Science.
[28] Assaf, H.S., et al., Geological, geochemical and mineralogical studies on the radioactive minerals occurrence at Qash Amir area, South Eastern Desert, Egypt. . J. Mineral Soc. Egypt, 1999. **11**: p. 135-156.
[29] Ibrahim, M.E., et al. El sella shear zone, southeastern Desert, Egypt; An example of vein-type uranium deposit. in 9 th Inter Min Petrol and Metall Eng Conf., . 2005. Cairo, Egypt.
[30] Abdalla, H.M., Geochemical and mineralogical studies at Um Ara rare metals prospect, Southeastern Desert, Egypt. 1996 Hokkaido University, : Japan.
[31] Roz, M.E., Geology and uranium mineralization of Gebel Gatter area, North Eastern Desert, Egypt. 1994, Al Azhar Univ,: Egypt. p. 175.
[32] Ibrahim, M.E., et al., Abu Rusheid lamprophyre dikes, South Eastern Desert, Egypt: as physical-chemical traps for REEs, Zn, Y, U, Cu, W, and Ag. . Arab J. Geosci., 2015. **8**: p. 9261-9270.
[33] Finch, R. and T. Murakami, Systematics and paragenesis of uranium minerals. 1999.
[34] Min, M.-Z., et al., Organic geochemistry of paleokarst-hosted uranium deposits, South China. 2000. **68**(3): p. 211-229.

[35] Chiozzi, P., V. Pasquale, and M.J.R.M. Verdoya, Naturally occurring radioactivity at the Alps–Apennines transition. 2002. **35**(2): p. 147-154.
[36] Tzortzis, M., et al., Gamma radiation measurements and dose rates in commercially-used natural tiling rocks (granites). 2003. **70**(3): p. 223-235.
[37] Amer, O., et al., Geochemical insight into granite hosted U-rich fluorite, Gabal El-Erediya area, Central Eastern Desert, Egypt: REE geochemical and fluid inclusion aspects. 2021. **14**(13): p. 1-17.
[38] Attawiya, M.Y., On the geochemistry and genesis of the uranium mineralization of El-Missikat area, Egypt Ann. Geol. Surv. Egypt 1984. **13**: p. 1–13.
[39] Hussein, H.A., et al., Uranium bearing silicious veins in younger granites, Eastern Desert, Egypt. 1986: Int. Atomic Energy Agency Report. p. 143 - 157.
[40] Hussein, H.A., M.A. El-Tahir, and A. and Abu Dief, Uranium exploration through exploratory mining work, south Qena-Safaga midway, Eastern Desert, in Egypt 3 rd Mining, Petrol. and Metal. Conf. 1992: Cairo Univ.,. p. pp. 92 - 105.
[41] Osmond, J.K., A.A. Dabous, and Y.H. and Dawood, Uranium series age and origin of two secondary uranium deposits, Central Eastern Desert, Egypt ,. Econ. Geol., 1999. **Vol. 94**: p. pp. 273 - 280.
[42] EL Kassas, I.A., Radioactivity and geology of Wadi Atalla area, Eastern Desert of Egypt, A.R.E. 1974, Fac. of Sci., Ein Shams Univ., Cairo, Egypt.
[43] Mohamed, N.A., Mineralogical and petrographical characteristics of some alteration products related to uranium mineralization in El-Missikat- El-Erediya areas, Eastern Desert, Egypt. 1988, Faculty of Science, Cairo Univ. p. 118 p.
[44] Bakhit, F.S. and I.A. El-Kassas, Distribution and orientation of radioactive veins in El-Erediya and El-Missikat, Central Eastern Desert, Egypt, in Int. Remote Sensing. 1989: Pristol Univ. p. pp. 565 - 581.
[45] Assran, A.S.M., Application of mining geophysical methods in the study of surface and subsurface geology of El-Erediya uranium prospect, Central Eastern Desert, Egypt. 1993, Ain Shams Univ. p. 177 p.
[46] Omran, A.A., Subsurface geologic studies of Gabal El-Eredyia uranium occurrence, Central Eastern Desert, Egypt. 1999, South Valley Univ. p. 136 p.
[47] Abdallah, S.M., Geological and mineralogical studies on some surface and subsurface sections from El-Missikat and El-Erediya uranium occurrences, Central Eastern Desert, Egypt. 2004, Ain Shams Univ. . p. 219p.
[48] Stern, R.J., Arc assembly and continental collision in the Neoproterozoic East African Orogen: implications for the consolidation of Gondwanaland. J. Annual Review of Earth Planetary Sciences, 1994. **22**(1): p. 319-351.
[49] Genna, A., et al., Proterozoic tectonism of the Arabian Shield. 2002. **117**(1-2): p. 21-40.
[50] Omran, A.A., et al., EL-MISSIKAT-EL EREDIYA URANIUM DEVELOPMENT PROJECT, EL EREDIYA AREA. 2014: Internal Report in the NMA, Egypt. p. 60.
[51] Matolin, M.M., Construction and use of spectrometric calibration pads, in Laboratory of Gamma-ray spectrometry. 1991, NMA: Egypt. p. 030-03.
[52] Mohamed, F.H., The role of the restite-unmixing and restite remelting processes in the evolution of the post-collision and anorogenic alkaline granites, Safaga area, Egypt: Geochemical and petrogenetic implications., in M.E.R.C. 1999, Earth Sc.Ser.: Ain Shams Univ., . p. 1-37.
[53] De la Roche, H., et al., A classification of volcanic and plutonic rocks using R1-R2 diagrams and major-element analyses-Its relation with current nomenclature. Chem. Geol. , 1980. **29**: p. 183-210.
[54] Taylor, S.R. and S.M.J.R.o.g. McLennan, The geochemical evolution of the continental crust. 1995. **33**(2): p. 241-265.
[55] Stempork, M., Mineralized granites and their origin. Episodes 1979 **3**: p. 20–24.
[56] Abdalla, H.M., Geochemistry and origin of rare metal mineralization of Um Safi felsite, Centeral Eastern Dessert, Egypt. Egyp. Jour.Geol. , 2001 **45(1A)**: p. 131–149.
[57] El-Kammar, A.M., et al., Geochemical constraints on rare metals mineralization at the central Eastern Desert of Egypt Geochem. J., 2001. **35,2**: p. 117–135.
[58] Brown, G.C., R.S. Thorpe, and P.C. Webb, The geochemical characteristics of granitoids in contrasting arcs and comments on magma sources. 1984. **141**(3): p. 413-426.
[59] Herrmann, A.G., Yttrium and lanthanides. . In: Handbook of geochemistry,. Vol. II. 1970, K. H Wedepohl (ed.),: Springer-Verlage, Berline
[60] Hanson, G.N., The application of trace elements to the petrogenesis igneous rocks of granitic composition. Earth Planet. Sci. , 1978. **Lett. 38**: p. 26-48.
[61] Lee, S.G., et al., Geochemical significance of the Rb–Sr, La–Ce and Sm–Nd isotope systems in A-type rocks with REE tetrad patterns and negative Eu and Ce anomalies: The Cretaceous Muamsa and Weolaksan granites, South Korea. Chemie der Erde – Geochemistry, 2013. **73**: p. 75-88.
[62] Irvine, T.N. and W.R.A. and Baragar, A guide to the chemical classification of the common volcanic rocks. Cana. J. Earth Sci. , 1971. **8,**: p. 523-548.
[63] Peccerillo, A. and S.R. Taylor, Geochemistry of Eocene calc-alkaline volcanic rocks from the Kastamonu area, Northern Turkey. . Contributions to Mineralogy and Petrology, 1976. **58**: p. 63-81.
[64] Maniar, P.D. and P.M.J.G.s.o.A.b. Piccoli, Tectonic discrimination of granitoids. 1989. **101**(5): p. 635-643.
[65] Chappell, B.W., A.J.E. White, and E.S.T.o.t.R.S.o. Edinburgh, I-and S-type granites in the Lachlan Fold Belt. 1992. **83**(1-2): p. 1-26.

[66] Whalen, J.B., K.L. Currie, and B.W. Chappell, A-type granites: geochemical characteristics, discrimination and petrogenesis. . Contributions to Mineralogy and Petrology 1987. **95**: p. 407–419.

[67] Eby N.G., Chemical subdivision of the A-type granitoids, Petrogenetic and tectonic implications. . Geology,, 1992. **20**: p. 641-644.

[68] Grebennikov, A.V., A-type granites and related rocks: Petrogenesis and classification. Science Direct, Russian Geology and Geophysics,, 2014. **55**: p. 1074-1086.

[69] Boynton, W.V., Geochemistry of Rare Earth Elements: Meteorite studies. . Rare Earth Elements Geochemistry., ed. P. In : Henderson, Ed.,. 1984, New York: Elsevier.

[70] Pearce, J.A., N.B.W. Harris, and A.G. Tindle, Trace element discrimination diagrams for the tectonic interpretation of granitic rocks. . J. Petrol., 1984. **25**: p. 956-983.

[71] Petro, W.L., T.A. Vogel, and J.T. and Wilbant, Major element chemistry of plutonic rock suites from compressional and extensional boundaries. . Chem. Geol., 1979. **26**: p. 216-235.

[72] Rogers, J.W. and J.K. Greenberg, Trace elements in continental margin magmatism: part 111, Alkali-granites and their relationship to cratonization: Summary. Geol. Soc. Am. Bull., 1981. **92**: p. 6-9.

[73] Batchelor, R.A. and P. Bowden, Petrogenetic interpretation of granitoid rock series using multicationic parameters. Chem. Geol., 1985. **48,**: p. p. 34-55.

[74] Laurent, O., et al., The diversity and evolution of late-Archean granitoids: Evidence for the onset of "modern-style" plate tectonics between 3.0 and 2.5 Ga. . Lithos 2014. **205,.** p. 208-235.

[75] Tuttle, O.F. and N.L. and Bowen, Origin of granite in the light of experimental studies in the system NaAlSi3¬O8-KAlSi3O8-SiO2-H2O. Geo. Soc. Am. , 1958. **Mem. 74,**: p. 1-146.

[76] Luth, W.C., R.H. Janns, and O.F. and Tuttle, The granite system at pressure of 4 to 10 kilobars. .J. Geophys. Res. , 1964. **69**: p. 759-773.

[77] James, R.S. and D.L. Hamilton, Phase relations in the system NaAlSi3O8–KAlSi3O8–CaAl2Si2O8–SiO2 at 1 kilobar water vapour pressure. Contributions to Mineralogy and Petrology 1969. **21,**: p. 111–141.

[78] Condie, K.C., . Archean magmatism and crustal thickening. . Geol. Soc. Am. Bull. , , 1973. **84**: p. 2981–2992.

[79] Manning, D.A.C., The effect of fluorine on liquidus phase relationship in the system Qz-Ab-Or with excess water at 1 kb. Contrib. Mineral. Petrol 1981. **76**: p. 206–215.

[80] Tutlle, O.F. and N.L. Bowen, Origin of granite in the light of experimental studies in the system $NaAlSi_3O_8$-$KAlSi_3O_8$-SiO_3-H_2O. [J]. Geol. Soc. Am. Mineral. , 1958. **74**: p. 153p.

[81] Winkler, H.H.F., M. Boese, and T. Marcopoulos, Low temperature granite melts. Neues Jahrb. Mineral. Montsh,, 1975.: p. 245–268.

[82] Meyer C and J.J. Hemely, Wall Rock Alteration. In geochemistry of Ore Deposits. in (ed. H.L. Barnes) [M]. 1967, New York. 166-235.

[83] Le Maitre, R.W., et al., A classification of igneous rocks and glossary of terms: Recommendations of the International Union of Geological sciences submisson on the systematics of igneous rocks: . 1989, USA: Oxford, Black-Well Scientific Publication.

[84] Clark S. Jr., Peterman J. E., and and Heier K. S., Abundance of uranium, thorium and potassium. In Handbook of Physical Contents (ed. Clark Jr. S. P.). Geol. Soc. Am. . Vol. Mem. 97. 1966.

[85] Adams, J.A., J.K. Osmand, and J.I.W. and Rogers, The geochemistry of thorium and uranium. In: Physics and chemistry of the earth. Vol. 3. 1956, New York: Pergamon Press.

[86] Turekian, K.K. and K.H. and Wedepohl, Distribution of elements in some major units of earth's crust. . Geol. Soc. Amer. Bull., 1961. **72,**: p. 175-190.

[87] Hussein A.H., Lecture Course in Nuclear Geology. , in Unpublished Internal Report,. 1978, Nuclear Materials Authority: Cairo, Egypt.

[88] El-Galy, M.M., Geology, Radioactivity, Geochemistry and Tectonic Setting of Selected Granitic Rocks, West Gulf of Aqaba, Sinai, Egypt. 1998: Tanta Univ., Egypt. p. 324.

[89] Surour A.A., et al., Geochemistry of wall rock alterations and radioactive mineralization in the vicinity of Hangaliya auriferous shear zone, Eastern Desert, Egypt. Egyptian Journal of Geology 2001. **45**: p. 187–212.

[90] Darnely, A.G., "Hot granites" Some general remarks, In: Maurice, Y.J. (ed.), Uranium in granites. Geol. Surv. Canada,, 1982. **paper No. 81-23,**: p. 1-10.

[91] Ragland, P.C., G.K. Billings, and J.A.J.G.e.C.A. Adams, Chemical fractionation and its relationship to the distribution of thorium and uranium in a zoned granite batholith. 1967. **31**(1): p. 17-33.

[92] Whitfield, J.M., J. Rogers, and J. Adams, The relationship between the petrology and the thorium and uranium contents of some granitic rocks. J. Geochimica et Cosmochimica Acta, 1959. **17**(3-4): p. 248-271.

[93] Larsen E.S. and D. Gottfried, Uranium and thorium in selected suites of igneous rocks. Am. J. Sci., 1960. **258**: p. 151–169.

[94] Falkum T. and Rose-Hansen J., The application of radioelement studies in solving petrological problems of the Precambrian intrusive Homme granite in the Lockeford area, South Norway. Chemical Geology, 1978. **23**: p. 73–86.

[95] Heinrich, E.W., Mineralogy and geology of radioactive raw materials. 1962: Mc Graw-Hill Book Company, New York.
[96] Gorman, D.H. and E.W. and Nuffield, : , , Studies of radioactive compound: uranophane and beta-uranophane. . Am. Min., 1955. **40**: p. 634- 645.
[97] Korzeb, S.L., The chemical evolution and paragenesis of uranium minerals from the Ruggles and Palermo granpegmatites, New Hampshire. Canadian Mineralogist., 1997. **35**: p. 135 - 144.
[98] Jefferies, N.L., The distribution of the rare earth elements within the Carnmenellis pluton, Cornwall. Mineralogical Magazine, 1984. **49**: p. 495-504.
[99] Deer, W.A., R.A. Howie, and J. and Zussman, Harlow, Essex, England: , :, An introduction to the rockforming minerals. (Second edition). 1992, Harlow, Essex, England: New York, NY: Longman Scientific.
[100] Mitchell, R.S., Metamict minerals: A review. Pt. I, Chemical and physical characteristics, occurrence. Pt. II, Origin of metamictization, methods of analysis, miscellaneous topics. . Mineral. Rec., 1973. **4,**: p. 214 -223.
[101] Dawoud, M., ,, The nature and origin of U-bearing fluids as revealed from zircon alteration: examples from the Gattarian granites of Egypt., in 6th Intern. Conf. On geochemistry, . 2004: Alex. Univ., Egypt. p. 875-891.
[102] EL-Kammar, A.M., et al., Geochemistry of accessory minerals associated with radioactive mineralization in the Central Eastern Desert, Egypt. . Journal of African Earth Sciences, 1997. **25/2,**: p. 237-252.
[103] Armbruster, T., et al., European Recommended nomenclature of epidote-group minerals. . J. Mineralogy,, 2006. **18**: p. 551-567.
[104] Wood, S.A. and A. Ricketts, Allanite-(Ce) from the Eocene Casto granite, Idaho: Response to hydrothermal alteration. . Canad. Mineral.,, 2000. **38**: p. 81-100.
[105] Hazen, R.M., R.C. Ewing, and D.A. and Svergensky, Evolution of uranium and thorium minerals. Am. Miner. , 2009. **94,**: p. 1293-1311.
[106] Berger, A., et al., Formation and composition of rhabdophane, bastnasite and hydrated thorium minerals during alteration: Implications for geochronology and low-temperature processes. . Chem. Geol. , 2008. **254,**: p. 238-248.
[107] Schandl, E.S. and M.P. and Gorton, A textural and geochemical guide to the identification of hydothermal monazite : criteria for selection of samples for dating. epigenetic hydrothermal ore deposits, 2004. **99(5),**: p. 1027-1035.
[108] Tischendorf, G., Geochemical and petrographic characteristics of silicic magmatic rocks associated with rare-element mineralization.In: Stemprock, M., Burnol, L. and Tiscendorf,G., Eds., Metallization Associated with acid magmatism, Czech. Geo. Surv.. 1977, Prague. 41-98.
[109] Heinrich, G.W., Mineralogy of radioactive raw materials. 1958, New York: McGraw Hill Book Co. 654p.